

The Fission Barrier of Heaviest Nuclei From a Macroscopic-Microscopic Perspective

Michał Kowal* and Janusz Skalski

Abstract The concept of fission barrier - a parameter which enters in quantitative estimates of various observables related to nuclear fission - is presented from the point of view of theory based on the picture of nuclear deformation and energy dependent on it. We describe the macroscopic-microscopic method of calculating energy landscapes which is simpler than the selfconsistent mean field approach, and, due to its two-component nature, seems to be easier to adjust to experimental data. We present some models and methods used to find the fission saddles. For the purpose of illustration, we present results on fission barriers in actinides and superheavy nuclei, obtained within one macroscopic-microscopic model. We discuss comparisons with results of other models, including some of the mean-field type.

Introduction

One of the most interesting subjects in the contemporary nuclear physics is the existence and stability of the heaviest atomic nuclei sometimes called superheavy. Since nuclear fission is one of their dominant decay channels, determining the main characteristics of this process is indispensable to estimate their half-lives.

Nearly immediately after its discovery, nuclear fission, both induced by neutrons [1] and spontaneous [2], was interpreted in analogy to the process of cell division in biology [3]. Atomic nucleus was represented as a drop of liquid [4, 5], after [6].

Michał Kowal

National Centre for Nuclear Research, Pasteura 7, 02-093 Warsaw, Poland, e-mail: michal.kowal@ncbj.gov.pl

Janusz Skalski

National Centre for Nuclear Research, Pasteura 7, 02-093 Warsaw, Poland, e-mail: janusz.skalski@ncbj.gov.pl

* corresponding author

The process itself was imagined as an increase in deformation under the disruptive electrostatic repulsion that, in spite of the counteracting nuclear attraction, eventually leads to scission. The notion of the fission barrier came about by imagining potential energy surface resulting from those forces and understood as a function of shape, or deformation q , of a drop of "nuclear matter". The energy surface should have a minimum at the deformation corresponding to the ground state (g.s.) of a nucleus and show a barrier along any path connecting it with a configuration of two nascent fragments, beyond which the potential should decrease with their distance, see Fig. 1. Along any path connecting the ground state with one of possible scission points there would be a point of maximal energy, V_{max} . The minimum over all such paths of the differences $V_{max} - E_{g.s.}$, with $E_{g.s.}$ the ground state energy, is the fission barrier height B ,

$$B = \min_{\text{paths}} \{V_{max} - E_{g.s.}\}. \quad (1)$$

It corresponds to some $V(q_{\text{saddle}})$ where q_{saddle} designates deformation of the saddle point.

Theoretical models giving energy of a nucleus as a function of its shape belong to the selfconsistent mean-field variety, either the Hartree-Fock (HF) or Hartree-Fock-Bogolyubov (HFB - when accounting for pairing correlations) formalism using some effective nucleon-nucleon (usually density-dependent) interaction or a density functional (if there is no underlying Hamiltonian). There exist also a relativistic alternative of the mean field theory in the form of Relativistic Mean Fields or Relativistic Hartree-Bogolyubov formalism. The fundamental quantities in such theories are single-particle neutron and proton densities which are constructed from eigenstates (orbitals) of the single-particle mean-field Hamiltonian whose eigenvalues are the single-particle energies. The HF(B) procedure, usually by means of energy minimization, gives one solution - the ground state or some other local energy minimum. A way to obtain the energy landscape consists in applying constraints when minimizing energy - energy map arises from many repeated calculations with varying constraints. The one-body densities provide deformation or shape parameters through their spatial moments: quadrupole, octupole, hexadecapole etc., defined in the center-of-mass frame of the nucleon density. At present, such theories are the most advanced of practically possible ones for the heaviest nuclei. They are covered by the N. Schunck contribution to this volume.

The purpose of this chapter is to familiarize the reader with a hybrid but quite effective method that allows estimating/determining the fission barrier B for heavy and superheavy nuclei. It is called the Macroscopic - Microscopic method (MM), as the calculation is divided into two parts: the macroscopic part involves most of the binding energy which has a smooth variation with Z and N ; the microscopic part involves a sum of individual nucleon contributions, showing oscillations with Z and N coming from the shell structure.

First, we present a general view on the fission process and our general understanding of it according to the excitation energy available to the decaying system, which points to the importance of the fission barrier. Then we present the shell correction method in connection to the mean-field theory. We discuss some models

describing the macroscopic energy and phenomenological single-particle potentials. The numerical diagonalization of the s.p. Hamiltonian including this potential delivers the s.p. spectra, to which the shell correction method can be applied. Then we discuss the selection of collective variables which build deformation space used in calculations and specific difficulties of a search for saddles in multidimensional spaces. Finally, the results of the MM method concerning fission barriers in actinides and superheavy nuclei are illustrated on the example of one specific model. We provide also some comparisons to experimental data and results of other MM and selfconsistent models.

General view of the fission process - the importance of the fission barrier

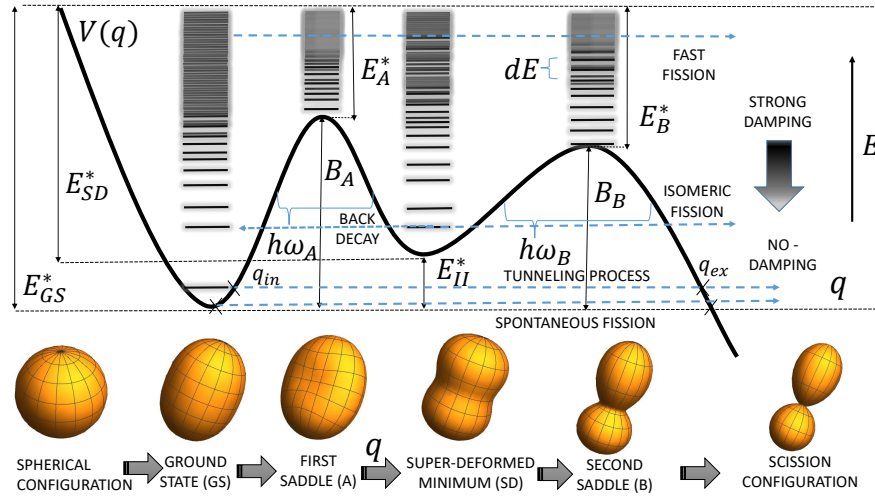


Fig. 1 Schematic one-dimensional picture of a double-humped fission barrier typical of actinides along the effective deformation parameter q . The index $A(B)$ stands for the first (second) saddle while $GS(SD)$ for the first (second) minimum. The fission barrier heights $B_{A(B)}$ and curvatures $\hbar\omega_{A(B)}$ are indicated. Densities of states and nuclear shapes corresponding to minima, saddles and a possible shape at the scission point are depicted below.

Although the fission barrier heights B are not directly measurable quantities, i.e. they are not quantum observables, they are very useful in estimating nuclear fission rates. As the activation energy E_a (per mole) in chemistry gives a rate k of a chemical reaction at temperature T via the Arrhenius law: $\Gamma = Ae^{-E_a/RT}$ (R - the gas constant; A - the frequency factor) [7, 8], the fission barrier gives the fission rate Γ^{fiss} of an

excited (as they usually are in nuclear reactions) nucleus via: $\Gamma^{fiss} \sim e^{-B/T_{eff}}$, where T_{eff} is an effective temperature (in energy units) derived from the excitation energy.

Let us give a few examples of nuclear reactions, to the analysis of which enters the fission barrier - that is, the "activation" threshold for the fragmentation of the nucleus into two fragments:

- the competition between neutron emission from, and fission of, a compound nucleus in fusion-fission reactions which determines the survival probability of the evaporation residue i.e. the probability that a superheavy nucleus will be created. This probability ratio is extremely sensitive to changes in B ;
- the growth of the total cross sections for the formation of the superheavy nuclei around $Z=118$;
- the competition between fission and other decay modes in the neutron capture reactions on neutron-rich nuclei lying on the path of the so-called r -process of the nucleosynthesis;
- fission barriers enter to the codes estimating induced fission cross-section as a function of energy, relevant to the reactor physics;
- spontaneous fission in which not only B alone, but the whole energy landscape, together with the mass parameters, determine fission half-lives.

A non-observable status of the fission barrier, again in analogy to that of the activation energy in chemistry, is reflected in its possible dependence on the reaction type and the excitation energy (effective temperature) range. This leads to some uncertainty in the calculations of fission barriers.

One can imagine an excited nucleus as a set of nucleons bouncing from walls of the slowly changing selfconsistent mean potential. The motion of the walls results from averaged motions of all nucleons and is 1-3 orders of magnitude slower than them. Separating slow, collective degrees of freedom of the potential walls from the fast ones, derived from motions of single nucleons, was never exactly accomplished in nuclear physics. Nevertheless, it is used in various simplified models to describe reactions like fission.

Within the mean-field theory, the wave function of a nucleus is assumed as a product state of individual nucleons occupying orbitals of the selfconsistent potential which depends on collective coordinates, denoted q . Take as q , for example, the elongation of a nucleus. Energies of s.p. states as functions of q have many avoided crossings between the g.s. and scission. Occupations of s.p. orbitals which at each q correspond to the lowest energy of a nucleus are called adiabatic, and in the HF it means that nucleons occupy the lowest orbitals. For a nucleus elongating with a velocity $\dot{q} > 0$ some nucleons may not follow adiabatic occupations at level crossings. If a nucleon occupies the same upsloping level through the crossing one says that its behaviour is diabatic. The uncertainty as to the adiabatic or diabatic character of crossings in fission directly translates into an uncertainty in the fission barrier height B . This problem concerns also activation energy in chemical reactions.

For an idealized isolated crossing of two levels with constant and opposite slopes $d\varepsilon/dq$, the interaction V , and at constant velocity \dot{q} , there is an exact solution for the probability that the particle occupying at time $t \rightarrow -\infty$ the lower adiabatic level

$E_1 = \frac{1}{2}[(\epsilon_1 + \epsilon_2) - \sqrt{(\epsilon_2 - \epsilon_1)^2 + 4V^2}]$ will occupy the upper adiabatic level $E_2 = \frac{1}{2}[(\epsilon_1 + \epsilon_2) + \sqrt{(\epsilon_2 - \epsilon_1)^2 + 4V^2}]$ at $t \rightarrow \infty$ [9]:

$$P = \exp\left(-\frac{2\pi}{\hbar} \frac{V^2}{\dot{q} \left| \frac{d}{dq}(\epsilon_2 - \epsilon_1) \right|}\right). \quad (2)$$

One should notice that the jump to the upper adiabatic state means that the crossing is *diabatic* - the particle will end in the state with the same slope. Generalizing this particular case one might say that a large interaction V , a small velocity \dot{q} and small relative slope $|d/dq(\epsilon_2 - \epsilon_1)|$ help to keep adiabatic configuration, while the opposite conditions enhance diabatic continuation [9, 10, 11, 12]. However, one should realize that the real processes last for a finite time, level slopes and the velocity change and consecutive crossings can interfere. Adiabatic vs diabatic scenario is

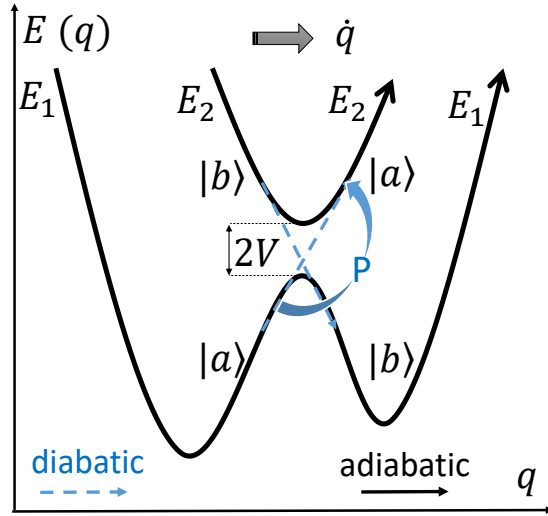


Fig. 2 Diabatic (blue arrow and dashed lines) vs. adiabatic (black lines) transition at the crossing of adjacent adiabatic levels E_1 and E_2 with the minimal distance $2V$.

schematically illustrated in Fig. 2 for two adiabatic energy levels E_1 and E_2 which exchange quantum characteristics of noninteracting states $|a\rangle$ and $|b\rangle$ in the region of crossing. The diabatic tendency to preserve level characteristics, including quantum numbers, is indicated by the blue arrow, and the adiabatic one, with the residual interaction leading to their exchange, by the black lines. A difference between the diabatic and adiabatic scenario is especially relevant for odd-A and odd-odd nuclei. It seems that for them, the sharp crossings of levels occupied by the odd particle

exclude the strictly adiabatic scenario. It is known that the diabatic effect of conserving the K quantum number (projection of the angular momentum of a nucleus on its symmetry axis) leads to a large increase in the calculated fission barriers, see, e.g., [13]. Unfortunately, there is no sufficiently reliable theory that would predict the importance of diabatic effects.

For the sake of further discussion we will distinguish three regimes according to the excitation energy of a nucleus. In particular, the induced fission with $E_{GS}^* \gg B_{A(B)}$ should be separated from the spontaneous one occurring from the ground state. Only in these extreme cases, when the energy is either much higher than the barrier height (then the details of the barrier do not actually matter much) and when we are dealing with the quantum tunneling deep under the barrier, one can treat fission as a one-step process. The region of the excitation energy just above the first or second saddle or not much smaller than them seems the most difficult to describe. There is no fundamental theory for the fission process in this energy regime. On the other hand, it is crucial from the point of view of applications e.g. in the reactor physics. Different mechanisms of fission depending on the energy available to the system are illustrated in Fig. 1. The fission barrier $B_{A(B)}$ helps in the understanding of each of them.

Regime: $E_{GS}^* \gg B_{A(B)}$ - statistical limit

In 1938 E. Wigner introduced Transition State Formalism (TSF) to calculate chemical reaction rates [14]. Later Bohr and Wheeler [5] realized that this formalism may be used to estimate the fission probability and that this process is mainly governed by the number of states above the fission barrier.

Due to differences in the shape of the nucleus, the energy levels above the fission barrier and above the ground state are distributed differently. For the excitation energy well above the *highest saddle point* the TSF predicts the fission decay width by integrating the density of states: $\rho_{A(B)}(E_{A(B)}^* - E)$ in the energy window: $E_{A(B)}^* = E_{GS}^* - B_{A(B)}$ (see Fig. 1):

$$\Gamma_{A(B)}^{fiss}(E_{GS}^*) = \frac{1}{2\pi\rho(E_{GS}^*)} \int_0^{E_{A(B)}^*} \rho_{A(B)}(E_{A(B)}^* - E) dE. \quad (3)$$

Here, $\rho(E)$ denotes the density of states of a nucleus at given deformation as a function of energy. The fission rate is controlled mainly by the height of the fission barrier $B_{A(B)}$ as it determines the upper limit of the integration in Eq. (3), that is, the energy window containing the appropriate number of nuclear states.

In the microcanonical ensemble the logarithm of the phase-space volume of the excited nucleus defines the entropy [15], while its derivative with respect to energy gives the level density (for simplicity here: $\rho_{A(B)}(E_{A(B)}^* - E) = \rho$):

$$\rho = e^S \frac{dS}{dE^*} \Rightarrow T = \overrightarrow{\frac{dE^*}{dS}}|_{V=const} \Rightarrow \rho = \frac{e^S}{T}. \quad (4)$$

We obtain this relationship by using the Maxwell relation for the thermodynamic potentials assuming the volume conservation during the process (in nuclear physics temperature is measured in energy units). Using the Fermi gas approximation (with the constant level density parameter a) which is reasonable for the excitation energy high above the barrier one has: $S = 2aT$ and $E^* = aT^2$. Inserting these into equation Eq. (3) and (4) we obtain (with the accuracy of the integration constant) the following expression for the fission rate:

$$\Gamma_{A(B)}^{fiss} \sim \frac{e^{S_{A(B)}} - 1}{e^{S_{GS}}}. \quad (5)$$

Since $S_{A(B)} \gg 1$, we have:

$$\Gamma_{A(B)}^{fiss} \sim e^{2\sqrt{aE_{A(B)}^*} - 2\sqrt{aE_{GS}^*}} \Rightarrow \Gamma_{A(B)}^{fiss} \sim e^{2\sqrt{a(E_{GS}^* - B_{A(B)})} - 2\sqrt{aE_{GS}^*}}. \quad (6)$$

For $E_{GS}^* \gg B_{A(B)}$ one can write:

$$\sqrt{a(E_{GS}^* - B_{A(B)})} - \sqrt{aE_{GS}^*} \approx \frac{-B_{A(B)}}{T}. \quad (7)$$

This led us to the Arrhenius rate-formula:

$$\Gamma_{A(B)}^{fiss} \sim \exp\left(-\frac{B_{A(B)}}{T}\right). \quad (8)$$

For low excitation energies, the assumption of an independent movement of nucleons is untenable, as the density of low-lying nuclear energy levels shows much structure.

The Eq. 8 is only valid for the angular momentum zero i.e. for the non-rotating nuclear system. For a non-zero angular momentum, assuming the axially symmetric shape at the saddle point, the rotational energy for the total angular momentum J and its projection onto symmetry axis K takes the form:

$$E_{rot}(J, K) = \frac{\hbar^2(J^2 - K^2)}{2J_{\perp}} - \frac{\hbar^2 K^2}{2J_{\parallel}}. \quad (9)$$

The saddle moments of inertia: perpendicular - J_{\perp} and parallel - J_{\parallel} to the symmetry axis, may be calculated from the rigid body model or treated as the empirical fit parameters. In a first approximation, one can simply add the rotational energy Eq. (9) at the ground state and at the saddle (different due to different deformations). A more refined recipe would be to add the rotational energy $E_{rot}(J, K)$ at each deformation and find the fission barrier depending on the angular momentum. Generally, as the moments of inertia increase with deformation, fission barrier decreases with J .

For high excitation energies, the phenomenon of dissipation begins to play an important role. H. Kramers was one of the first [16] to consider such dynamical corrections. Assuming the one-dimensional fission path [16], a parabolical shape for the ground state minimum (of curvature ω_{GS}), and an inverted parabola shape for the top of the barrier (with curvature $-\omega_{A(B)}$), one obtains, in the limit of large dissipation:

$$\Gamma_{diss}^{fiss} \simeq \frac{\omega_{GS}}{\omega_{A(B)}} \left(\sqrt{\frac{\gamma^2}{4} + \omega_{A(B)}^2} - \frac{\gamma}{2} \right) e^{\frac{-B_{A(B)}}{T}} \Rightarrow \gamma \gg \omega_{A(B)} \Rightarrow \Gamma_{overdamped}^{fiss} \simeq \frac{\omega_{A(B)} \omega_{GS}}{\gamma} e^{\frac{-B_{A(B)}}{T}}. \quad (10)$$

The condition ($\gamma \gg \omega_{A(B)}$) is called the overdamped limit. The friction coefficient γ controls the intensity of the stochastic forces $\eta(t)$ responsible for the interaction of the collective motion with the thermal bath of other degrees of freedom (the environment) via the autocorrelation function $\langle \eta(t) \eta(t') \rangle \approx \gamma T \delta(t - t')$. This stochastic force (based on rather heuristic arguments) is added to the conservative driving force $-\frac{dV(q)}{dq}$, giving a stochastic dynamic description of the fissioning system. At the limit of an overdamped stochastic process, the corresponding classical Langevin equation of motion has the form:

$$\gamma \frac{dq}{dt} = -\frac{dV(q)}{dq} + \eta(t). \quad (11)$$

The dissipative dynamics approach has proved very successful in modeling the fission process. There are a number of generalizations of this method due to many dimensions, different friction regimes or types of the stochastic noise. A broad overview can be found in [17, 18, 19, 20].

Regime: $E_{GS}^* \ll B_{A(B)}$ - quantum tunneling limit

The collective tunneling limit is usually treated in the quasiclassical approximation which leads to a WKB-type formula [21]. The fission rate up to subexponential corrections is given by:

$$\Gamma \approx P^{WKB} \approx e^{-2S(L)}, \quad (12)$$

where $S(L)$ is action integral:

$$S(L) = \int_{q_{in}}^{q_{ex}} \sqrt{\frac{2}{\hbar^2} \{M_L(q)[V_L(q) - E_0]\}} dq, \quad (13)$$

calculated along the optimal fission path L in a multi-deformation space, for which $S(L)$ is the smallest. The application of the variational principle makes it possible to find the optimal path. Here, $V_L(q)$ is the potential energy, $M_L(q)$ is the effective inertia along the trajectory L . E_0 is the initial energy of a fissioning nucleus. The parameter q specifies the position of a point on the trajectory L , with q_{in} and q_{ex}

corresponding to the entrance and exit points of the barrier, i.e., to the classical turning points determined by $V_L(q) = E_0$. These points are schematically shown in Fig. 1.

The effective inertia $M_L(q)$ associated with the fission motion along the trajectory L is usually calculated in the frame of the cranking approximation [22]. Because it goes beyond the scope of this chapter, we refer the reader to the book [23].

Regime: $E_{GS}^* \simeq B_{A(B)}$ - damping limit

One can try to understand physics in this limit or even calculate the corresponding effective tunneling coefficients based on the idea of the optical potential [21, 24, 25, 26]. The transmission through a multi-humped fission barrier depends on the degree of damping of the vibrational states in the potential minima. In the frame of this concept, the strong damping limit, marked in the Fig. 1 for energies close to B_A and B_B , means that the second minimum begins to absorb particles passing through it. A fraction of the particle stream not absorbed by the second minimum may pass further through the second barrier, usually different from the first one in its shape and height. These differences cause different probabilities of transmission over each of them. In the strong damping regime, assuming full absorption by the second minimum, one can write the average transmission ratio as:

$$\langle T \rangle \simeq \left[\frac{1}{T_A} + \frac{1}{T_B} \right]^{-1} \Rightarrow \langle T \rangle \simeq \frac{T_A T_B}{T_A + T_B}. \quad (14)$$

In this approximation, coefficients of transmission through successive barriers are independent of each other.

In practical calculations, the individual character of low-lying excited states should be taken into account. The discrete transition states (denoted here by the index d) are the rotational levels built on vibrational or non-collective band heads, characterized by a given set of quantum numbers (angular momentum J , parity π , and angular momentum projection on the nuclear symmetry axis K). We may assume that the fission process occurs through such analog states, i.e., retaining the quantum characteristics of the compound nucleus states. These so-called transition states are located on top of the appropriate saddle point, and due to their discrete nature, they should be separated from the continuous spectrum by assigning an individual probability of decay to each of them. In general, each such state has a specific fission barrier $B_{A(B)}^d$ and, consequently, the probability of penetration thereof. For nucleus energy above the barrier, $E_{GS}^* \geq B_{A(B)}^d$, one uses the Hill-Wheeler barrier transmission coefficient [10, 21]:

$$T_{A(B)}^{HL}(E) = \frac{1}{1 + \exp\left[\frac{2\pi(B_{A(B)}^d - E)}{\hbar\omega_{A(B)}}\right]}. \quad (15)$$

If available energy is below the barrier, $E_{GS}^* < B_{A(B)}^d$, then we can use the previously introduced tunneling probability P^{WKB} . Transmission coefficients $T_{A(B)}$, which one should then use in Eq. (14) are written in the following form:

$$T_{A(B)} = \sum_d P_{A(B)}^{HL(WKB)}(E) + \int_{E_d}^{E_{dA(B)}^*} P_{A(B)}^{HL(WKB)}(E) \rho_{A(B)}(E_{dA(B)}^* - E) dE. \quad (16)$$

Note that this time the integration takes place from a specific energy of the discrete state above the saddle (E_d) in the energy window defined by the diabatic barrier $B_{A(B)}^d$, characteristic for it, $E_{dA(B)}^* = E_{GS}^* - B_{A(B)}^d$. In this way we have extracted (following the authors [26]) a discrete part of the spectrum above the saddle. After normalizing to the density of the available states over the ground state, one obtains the average effective fission width in the over-damped regime:

$$\langle \Gamma^{fiss} \rangle = \frac{\langle T \rangle}{2\pi\rho(E_{GS}^*)}. \quad (17)$$

This is a heuristic and approximate, but pragmatic approach as it allows to calculate the probabilities of induced fission. Unfortunately, there is still no fundamental theory that would allow the reconstruction of cross-sections in this process, that are key for applications. The main reason for this state of affairs is the fact that we still do not know how to correctly calculate the fundamental quantity occurring in most of the integrals presented, namely the total density of nuclear states located both above the ground state and above the appropriate saddle. There are only a number of approximate methods to do this [27, 28, 29, 30, 31, 32, 33, 34, 35, 36, 37].

Macroscopic - Microscopic method

The macroscopic-microscopic method is an approximation to the full selfconsistent Hartree-Fock(-Bogolyubov) theory. It is based on the observation that differences between nuclear binding (or masses) and their liquid-drop model estimates oscillate with Z and N with the amplitude ≤ 10 MeV. The minima of these oscillations correspond to particularly stable magic nuclei. This difference, termed the shell correction, has its origin in the bunching of quantum s.p. levels i.e. the non-uniformity of the density of quantum s.p. states per energy interval. This genuinely quantum phenomenon occurs in many spectra and in the case of atomic nuclei leads to shells containing $\approx A^{2/3}$ states, with the energy distance between them of $\hbar\Omega \approx 5 - 10$ MeV. V. Strutinsky proposed a simple method to calculate shell correction [39, 40] based on the idea that a difference between the real binding energy and its value given by the liquid-drop formula could be expressed as a difference between the sums of single-particle energies in a phenomenological s.p. potential: one for the quantum one-body density and the other for the density averaged over shells. The averaging should eliminate shell non-uniformities, thus its energy range should be of the order

of $\hbar\Omega$. The averaged density of s.p. states should be close to the quasiclassical one, without shell oscillations, but reflecting a smooth increase in energy $\sim \sqrt{E - V_0}$ (with V_0 - the bottom of the potential well), characteristic of three-dimensional systems. Below, following M. Brack et al. 1972 [41], we present the shell correction method in connection to the mean-field theory.

Shell Correction vs the Mean Field

Energy of a nucleus in a state represented by a Slater determinant built out of single-nucleon states $|\phi_k\rangle$, with the Hamiltonian consisting of the kinetic energy \hat{t} and a two-body nucleon-nucleon interaction \hat{v} , $\hat{H} = \hat{t} + \hat{v}$, can be expressed as a function of the one-body density ρ which, when understood as an operator, can be written as:

$$\hat{\rho} = \sum_{n \text{ occ}} |\phi_n\rangle\langle\phi_n|, \quad (18)$$

with n - indices of the occupied orbitals. (The one-body density should not be confused with the energy density of states of the whole nucleus, customarily denoted by the same symbol in the preceding section.) In any orthogonal s.p. basis, we have:

$$E(\{\phi_k\}) = E(\rho) = \sum_{\mu\nu} t_{\mu\nu} \rho_{\nu\mu} + \frac{1}{2} \sum_{\mu\nu\gamma\delta} (v_{\mu\nu\gamma\delta} - v_{\mu\nu\delta\gamma}) \rho_{\delta\nu} \rho_{\gamma\mu}, \quad (19)$$

with $v_{\mu\nu\gamma\delta}$ - matrix elements of the interaction. The functional derivative of energy $E(\{\phi_k\})$ with respect to the complex-conjugate function ϕ_m^* equals:

$$\delta E(\{\phi_k\}) / \delta \phi_m^* = \hat{h}(\rho) |\phi_m\rangle, \quad (20)$$

where $\hat{h}(\rho) = \hat{t} + \hat{V}$ is the one-body Hamiltonian with the mean-field potential dependent on the density ρ , i.e. on the occupied orbitals:

$$V_{\mu\nu}(\rho) = \sum_{\gamma\delta} (v_{\mu\gamma\nu\delta} - v_{\mu\gamma\delta\nu}) \rho_{\delta\gamma}. \quad (21)$$

One-body density can be presented as a function: $\rho(\mathbf{r}, \mathbf{r}') = \langle \mathbf{r} | \hat{\rho} | \mathbf{r}' \rangle = \sum_n \phi_n(\mathbf{r}) \phi_n^*(\mathbf{r}')$. If some function $\rho(\mathbf{r}, \mathbf{r}')$ is a selfconsistent one-body density solution to the Hartree-Fock problem, there is a basis of s.p. states $|\phi_\mu\rangle$, a subset $|\phi_n\rangle$ of which forms the density ρ , that fulfil HF equations:

$$\hat{h}(\rho) \phi_\mu = (t + \hat{V}) \phi_\mu = e_\mu \phi_\mu, \quad (22)$$

with e_μ the HF s.p. energies. One can construct such solutions for various prescribed values of multipole moments which would correspond to various nuclear deformations.

A functional dependence of energy $E(\rho)$ on $\rho(\mathbf{r}, \mathbf{r}')$ can be considered generally even for functions which *do not represent any Slater determinant*. One can formally define the functional derivative $\delta E(\rho)/\delta \rho(\mathbf{r}, \mathbf{r}')$ as the matrix element of some one-body Hamiltonian $\langle \mathbf{r}' | \hat{h}(\rho) | \mathbf{r} \rangle$. With such a more general definition, a difference in energies calculated for such generalized densities, one $\rho^{(1)}$ and the other $\rho^{(2)}$, reads:

$$E(\rho^{(1)}) - E(\rho^{(2)}) = \text{Tr } \hat{h}(\rho^{(2)})(\rho^{(1)} - \rho^{(2)}) + \text{terms} \sim (\rho^{(1)} - \rho^{(2)})^2, \quad (23)$$

where, in any orthogonal basis, $\text{Tr } AB = \sum_{\mu\nu} A_{\mu\nu} B_{\nu\mu}$.

Now we consider a density $\tilde{\rho}$, obtained from ρ by a procedure of averaging over the shell structure, the details of which will be specified later. In a broad sense, one can think of $\tilde{\rho}(Z_0, N_0)$ as obtained by averaging one-body HF densities over a range of neutron and proton numbers N and Z around N_0 and Z_0 . It is assumed that the density $\tilde{\rho}$ is close to ρ , and the mean-field $\hat{h}(\tilde{\rho})$ is close to $\hat{h}(\rho)$, so that $\delta\rho = \rho - \tilde{\rho}$ and the difference in s.p. potentials $\delta V = \hat{h}(\rho) - \hat{h}(\tilde{\rho}) = V - \tilde{V} \sim \delta\rho$ are considered as small of the first order. In general, the density $\tilde{\rho}$ does not correspond to any Slater determinant so there are no orbitals building it and no HF equations which they would fulfil. Nevertheless, there is a basis of s.p. wave functions defined by the eigenequation:

$$\hat{h}(\tilde{\rho})\psi_\mu = (\hat{t} + \hat{V})\psi_\mu = \varepsilon_\mu \psi_\mu. \quad (24)$$

We interpret $\hat{h}(\tilde{\rho})$ as the *phenomenological s.p. Hamiltonian* and its eigenfunctions ψ_μ as the corresponding *phenomenological s.p. wave functions*. Those of them which correspond to occupied selfconsistent states ϕ_n define the *phenomenological s.p. density*, $\rho^S = \sum_{n \text{ occ}} |\psi_n\rangle\langle\psi_n|$. As $h(\rho) = h(\tilde{\rho}) + \delta V$, the difference between ϕ_v and ψ_v follows from the perturbation expansion:

$$|\phi_v\rangle = |\psi_v\rangle + \sum_{\mu \neq v} |\psi_\mu\rangle \frac{\langle\psi_\mu | \delta V | \psi_v\rangle}{\varepsilon_v - \varepsilon_\mu} + \dots \quad (25)$$

Since to the first order in δV : $\rho - \rho^S = \sum_{n \text{ occ}} |\delta\psi_n\rangle\langle\psi_n| + |\psi_n\rangle\langle\delta\psi_n|$, where $\delta\psi_n = \phi_n - \psi_n$, and $\langle\delta\psi_k | \psi_k\rangle = 0$, one obtains that $\text{Tr } \hat{h}(\tilde{\rho})(\rho - \rho^S)$ is of the second order in δV .

As the difference between ρ and ρ^S is in the first order proportional to δV , the difference between averaged densities, $\tilde{\rho}$ and $\tilde{\rho}^S$ would be proportional to the averaged δV . From the formula (21) for $V_{\mu\nu}(\rho)$ this is proportional to the averaged $\delta\rho$ and that is zero. Therefore, it is natural to expect that the difference $\tilde{\rho} - \tilde{\rho}^S$ is of the second order in $\delta\rho$.

Then, as $\delta\rho = (\rho - \rho^S) + (\rho^S - \tilde{\rho}^S) + (\tilde{\rho}^S - \tilde{\rho})$, it follows from the above that the difference between $\text{Tr } \hat{h}(\tilde{\rho})\delta\rho$ and $\text{Tr } \hat{h}(\tilde{\rho})(\rho^S - \tilde{\rho}^S)$ is of the second order in $\delta\rho$. Hence, from Eq. (23), substituting ρ for $\rho^{(1)}$ and $\tilde{\rho}$ for $\rho^{(2)}$, one obtains:

$$E_{HF}(\rho) - E(\tilde{\rho}) = \text{Tr } \hat{h}(\tilde{\rho})(\rho^S - \tilde{\rho}^S) + \text{terms} \sim (\delta\rho)^2. \quad (26)$$

This equation, sometimes called the Strutinsky energy theorem, is the basis of the shell correction method. It states that the selfconsistent HF energy may be presented as a sum of two terms: $E(\bar{\rho})$ which smoothly depends on Z and N and $\text{Tr } \hat{h}(\rho^S - \bar{\rho}^S)$ which exclusively derives from the *phenomenological*, deformation-dependent s.p. Hamiltonian and contains all the first order effects of the shell structure. More specifically, the first order effects of the shell structure are contained in the sum of s.p. energies of occupied phenomenological levels $\text{Tr } \hat{h}\rho^S$, as those in $\text{Tr } \hat{h}\bar{\rho}^S$ are at most of the second order in $\delta\rho$.

This lends argument to the following reasoning: If we replace the smoothed HF energy $E(\bar{\rho})$ by a liquid-drop energy E_{LD} , and assume that a phenomenological single-particle Hamiltonian \hat{h} has the same spectrum around the Fermi energy as $\hat{h}(\bar{\rho})$, we obtain to the first order in $\delta\rho$:

$$E_{HF}(\rho) \approx E_{LD} + \text{Tr } \hat{h}(\rho^S - \bar{\rho}^S) = E_{LD} + \delta E. \quad (27)$$

If we further adjust the parameters of the liquid-drop energy so that $E_{LD} + \delta E$ with a given phenomenological potential fit the experimental binding energies we may hope to incorporate the second order terms of the shell correction into E_{LD} and improve the overall description of data beyond the first order agreement of the Strutinsky energy theorem.

Calculation of the Shell Correction

To calculate the shell correction one uses the density of single-particle states of \hat{h} per energy interval which is just a sum of delta functions at single-particle energies, $g(\epsilon) = \sum_v \delta(\epsilon - \epsilon_v)$, and its smoothed version (defined below) $\tilde{g}(\epsilon)$:

$$\delta E = \int \epsilon (g(\epsilon) - \tilde{g}(\epsilon)) d\epsilon = U - \tilde{U}, \quad (28)$$

with:

$$U = \sum_v n_v \epsilon_v, \quad (29)$$

where n_v are occupation numbers (either 0 or 1), and

$$\tilde{U} = \int_{-\infty}^{\tilde{\lambda}} \epsilon \tilde{g}(\epsilon) d\epsilon. \quad (30)$$

The quantity $\tilde{\lambda}$ is the Fermi energy for the smoothed density, determined by the fixed number of particles. The whole procedure is made separately for neutrons and protons, and the shell correction is the sum of their separate contributions, $\delta E = \delta E_n + \delta E_p$. Hence the equation fixing $\tilde{\lambda}_n$ is:

$$N = \int_{-\infty}^{\tilde{\lambda}_n} \tilde{g}_n(\varepsilon) d\varepsilon, \quad (31)$$

and the analogous one fixes $\tilde{\lambda}_p(Z)$. Usually one assumes the Kramers degeneracy of s.p. levels and then one has sums over half of s.p. levels multiplied by 2.

The "smooth" density is not unique, but arguments can be made for choosing it in a form of convolution (folding) of the density $g(\varepsilon)$ with some smoothing function ξ with a width $\bar{\gamma} > \hbar\Omega$,

$$\tilde{g}(\varepsilon) = \frac{1}{\bar{\gamma}} \int_{-\infty}^{\infty} g(\varepsilon') \xi\left(\frac{\varepsilon - \varepsilon'}{\bar{\gamma}}\right) d\varepsilon' = \frac{1}{\bar{\gamma}} \sum_v \xi\left(\frac{\varepsilon - \varepsilon_v}{\bar{\gamma}}\right). \quad (32)$$

It follows from the finite width $\bar{\gamma}$ and the condition (31) that the shell correction is determined exclusively by the s.p. levels lying, roughly, not much farther than $\bar{\gamma}$ from the Fermi level.

Most often one takes for ξ a folding function f_p of the Gaussian type, being the formal expansion of the δ -function, truncated to the first p terms (with p even):

$$f_p(x) = \frac{1}{\sqrt{\pi}} \sum_{n=0}^p C_n H_n(x) e^{-x^2}, \quad (33)$$

with

$$C_n = \frac{1}{2^n n!} H_n(0) = \begin{cases} \frac{(-1)^{\frac{n}{2}}}{2^n (\frac{n}{2})!} & \text{for even } n \\ 0 & \text{for odd } n. \end{cases} \quad (34)$$

Then, one obtains the averaged density:

$$\tilde{g}(\varepsilon) = \frac{1}{\bar{\gamma}\sqrt{\pi}} \sum_v e^{-u_v^2} \sum_{n=0}^p C_n H_n(u_v), \quad (35)$$

with $u_v = (\varepsilon - \varepsilon_v)/\bar{\gamma}$.

The shell correction (28) is strongly correlated with the local density of states around the Fermi energy ε_F ; $\delta E > 0$ if there are more states there than it would follow from $\tilde{g}(\varepsilon_F)$, $\delta E < 0$ if there are less. The large negative δE stabilizes a particular deformation. Hence the energy gaps in the single particle spectrum signal possible stable configurations/deformations.

In general, energy \tilde{U} depends on the parameters $\bar{\gamma}$ and p . At the beginning, it seemed that for the method to be meaningful there should be certain interval of $\bar{\gamma}$ and corresponding p , for which \tilde{U} would not practically depend on them (the so called "plateau condition"), as it was found for the harmonic oscillator potential. However, later it turned out that:

- 1) The shell correction effectively depends on one parameter: $\bar{\gamma}/\sqrt{p}$ [48].
- 2) For finite-depth potentials the plateau condition usually does not hold. In addition, there is a strong and unrealistic dependence of δE on the positive energy spectrum which poses an acute problem for nuclei close to the neutron drip line [47, 49]. The method can be modified to practically overcome this problem [50, 51, 52, 48].

3) A reasonable condition is that \tilde{U} be close to the semiclassical energy, which, after properly taking care for the positive energy spectrum, happens for the smallest $\tilde{\gamma} > \hbar\Omega$ for which one obtains a monotonically increasing smoothed density $\tilde{g}(\epsilon)$ [49, 53].

4) In general, there remains a difference between \tilde{U} and the semiclassical energy, typically a few hundred keV, which depends on a nucleus and deformation ([49, 53]).

For the sake of a complete picture one should add at this point that the calculation of the semiclassical density and energy is much more cumbersome than that of the Strutinsky shell correction.

Pairing correction

The presence of the energy gap in spectra of even-even nuclei and the substantially less-than-rigid values of the moments of inertia observed in rotational bands are evidence for pair correlations in atomic nuclei. Most frequently they are included in theoretical models by adopting the BCS formalism from the theory of superconductivity. Usually it is assumed that a short-range attraction with a constant matrix element G acts between all pairs of time-reversed s.p. states. The schematic pairing hamiltonian, treated separately for neutrons and for protons, may be written as:

$$H = \sum_{\nu} \epsilon_{\nu} a_{\nu}^{\dagger} a_{\nu} - G \sum_{\nu, \bar{\nu} > 0} a_{\nu}^{\dagger} a_{\bar{\nu}}^{\dagger} a_{\bar{\nu}} a_{\nu}, \quad (36)$$

where, as before, ϵ_{ν} denotes the energy of a single-particle state ν . Each state ν has its time-reversal-conjugate $\bar{\nu}$ with the same energy (Kramers degeneracy). One assumes the BCS wave function for the nuclear ground state. As it is a superposition of components with different numbers of particles, one requires that the expectation value of the particle number has a definite value n ($n = N$ for neutrons and $n = Z$ for protons):

$$\langle \hat{n} \rangle = 2 \sum_{\nu > 0} v_{\nu}^2 = n. \quad (37)$$

The BCS occupation numbers are given by

$$v_{\nu}^2 = \frac{1}{2} \left[1 - \frac{(\epsilon_{\nu} - \epsilon_F)}{\sqrt{(\epsilon_{\nu} - \epsilon_F)^2 + \Delta^2}} \right], \quad (38)$$

where the parameters ϵ_F and Δ are solutions of the system of two equations, for the average particle number:

$$n = \sum_{\nu > 0} \left[1 - \frac{\epsilon_{\nu} - \epsilon_F}{\sqrt{(\epsilon_{\nu} - \epsilon_F)^2 + \Delta^2}} \right], \quad (39)$$

and for the pairing gap:

$$\frac{2}{G} = \sum_{v>0} \frac{1}{\sqrt{(\epsilon_v - \epsilon_F)^2 + \Delta^2}}. \quad (40)$$

The larger the number of s.p. states included in the summation in Eq. (40) the greater BCS solution for Δ is obtained. This follows from the unphysical assumption of the constant matrix element G . There are more refined choices of interactions producing pair correlations, but the simplest remedy is to fit pairing strengths to some data by using a prescribed number of included s.p. levels.

Energy of the system in the BCS state reads:

$$E_{BCS} = 2 \sum_{v>0} \epsilon_v v_v^2 - \frac{\Delta^2}{G} - G \sum_{v>0} v_v^4. \quad (41)$$

For nuclei with odd Z or N , one s.p. level is singly occupied. This level is excluded - blocked - when the BCS theory is applied to the remaining even number of particles.

Pairing correction energy δE^{pair} is constructed in analogy to the shell correction energy δE ,

$$\delta E^{pair} = E_{pair} - \tilde{E}_{pair}, \quad (42)$$

where E_{pair} is the pairing energy, i.e. energy difference between the paired and unpaired system, corresponding to real single-particle level distribution $g(\epsilon)$, and \tilde{E}_{pair} is such an energy difference for the smoothed single-particle level distribution, $\tilde{g}(\epsilon)$. One has: $E_{pair} = E_{BCS} - E_{BCS}^{\Delta=0}$, where $E_{BCS}^{\Delta=0}$ is the E_{BCS} energy in the limit of disappearing pairing correlations ($\Delta = 0$),

$$E_{BCS}^{\Delta=0} = 2 \sum_{v=1}^{n/2} \epsilon_v - \frac{Gn}{2}. \quad (43)$$

The smoothed pairing energy term \tilde{E}_{pair} is usually included in a schematic form, resulting from a model with the constant density of doubly degenerate energy levels. When calculated in such way, it shows nearly no deformation dependence. For example, it varies by about 50 keV over the whole deformation range in actinides. Thus, it could be omitted in energy landscapes, while it shows up in binding energies.

The pairing correction (42) counteracts the shell correction δE ; it is positive where the density of states around the Fermi energy is larger than average and negative in the opposite case. Therefore a stronger pairing diminishes the calculated fission barriers.

Some remarks on the macro-micro method

Concluding this short description of the macro-micro method one can notice that the micro and macro parts are to a large extent adjusted *separately*: the first one to the bulk, and the second one to the single-particle properties of nuclei. This makes the method theoretically incoherent but more flexible than the HF(B)/functional methods in which both types of properties are fixed once the effective interaction/functional is chosen. In effect, the fit to nuclear properties by selfconsistent models turns out more difficult, for example, a good fit to masses does not guarantee realistic fission barriers or s.p. levels similar to experimental ones. Moreover, self-consistent calculations are so much more laborious that the systematic (that means for many nuclei) and methodologically correct (that means: not relying on the energy minimization) determination of the fission saddles was for them impossible up to now.

The Strutinsky method over the last 50 years gave most of the predictions concerning nuclear deformations over the periodic table. Although it *does not* give the exact value of the HF(B) energy, the important observation is that, except for very neutron-rich nuclei, there were very few, if any, instances in which a macro-micro method based on a reasonable phenomenological potential would not reproduce robust landscape features predicted by reasonable selfconsistent calculations.

Choice of Models

A practical implementation of the macro-micro method will depend on choosing a specific model for the macro energy and for the phenomenological s.p. potential. Below we describe some most frequent choices.

Macroscopic Energy

The expression for nuclear binding energy as a smooth function of Z and N is motivated by the saturation property of nuclear forces and the idea of *leptodermous* expansion. From the experimentally measured nuclear masses we see that the binding energy is roughly proportional to the number of nucleons $A = Z + N$. From the electron scattering off nuclei we learn that proton densities of medium-mass and heavy nuclei A) show roughly constant surface diffuseness $b \approx 2.4$ fm understood as a radial distance between points where density falls from 90% to 10% of its central value and B) have radii following the $R \approx r_0 A^{1/3}$ dependence with $r_0 \approx 1.2$ fm. Hence the nuclear binding coming from the attractive nuclear force could be expanded in powers of $b/R \sim A^{-1/3}$ with consecutive terms depending on the geometrical properties of nuclear surface Σ , see e.g. [61]:

$$E_{nuc} = C_V A - C_S \oint_{\Sigma} dS - C_c \oint_{\Sigma} \kappa dS - C_G \oint_{\Sigma} \kappa_G dS + \dots, \quad (44)$$

where κ is the surface curvature, $\kappa = \frac{1}{2}(\frac{1}{R_1} + \frac{1}{R_2})$, with R_1 and R_2 principal radii of curvature, and the Gaussian curvature $\kappa_G = \frac{1}{R_1 R_2}$. For a spherical nucleus these terms are equal to: $C_S 4\pi R^2 \sim A^{2/3}$, $C_c 4\pi R \sim A^{1/3}$, and $C_G 4\pi \sim A^0$. The last term is shape-independent as $\oint_{\Sigma} \kappa_G dS$ is the topological invariant. The constants in this expansion are in fact functions of the neutron excess, $I = (N - Z)/A$, which should be even if we accept the charge symmetry of nuclear interactions. One can redefine constants so that the new ones will stand by the consecutive powers of $A^{1/3}$ multiplied by the corresponding surface integrals divided by their spherical values:

$$B_S(\Sigma) = \oint_{\Sigma} dS / (4\pi r_0^2 A^{2/3}); \quad B_{curv}(\Sigma) = \oint_{\Sigma} \kappa dS / (4\pi r_0 A^{1/3}). \quad (45)$$

One also has to add the Coulomb energy of proton repulsion, a large term for the heaviest nuclei. In the spirit of the expansion (44) its leading term is calculated for a constant proton density inside a sharp nuclear surface, $\rho_p(\mathbf{r}) = \rho_0 = -Ze/(4\pi R^3/3)$ inside Σ , and zero outside (with e - the elementary charge):

$$E_{Coul} = \frac{1}{2} \int \int \frac{\rho_p(\mathbf{r}) \rho_p(\mathbf{r}') d^3 \mathbf{r}' d^3 \mathbf{r}}{|\mathbf{r} - \mathbf{r}'|} \rightarrow \frac{\rho_0^2}{2} \int \int_{V_{\Sigma}} \frac{d^3 \mathbf{r}' d^3 \mathbf{r}}{|\mathbf{r} - \mathbf{r}'|}. \quad (46)$$

Gathering terms we obtain the liquid-drop formula:

$$\begin{aligned} E_{mac}(Z, N, \Sigma) = & a_v(1 - \kappa_v I^2)A - a_s(1 - \kappa_s I^2)A^{2/3} B_S(\Sigma) \\ & - a_c(I^2)A^{1/3} B_{curv}(\Sigma) - a_0 A^0 \\ & - c_1 Z^2 A^{-1/3} B_C(\Sigma) + c_4 Z^4 A^{-1/3} + \dots, \end{aligned} \quad (47)$$

where $c_1 = \frac{3}{5} \frac{e^2}{r_0}$, and $B_C(\Sigma)$ - a shape-dependent ratio of dimensionless Coulomb energies for the deformed and spherical nucleus:

$$B_C(\Sigma) = \frac{15}{32\pi^2 R^5} \frac{\int \int_{V_{\Sigma}} d^3 \mathbf{r}' d^3 \mathbf{r}}{|\mathbf{r} - \mathbf{r}'|}. \quad (48)$$

The last term in expression (47) is the quantal Coulomb-exchange term for a spherical nucleus in the Slater approximation. It is an example of deformation-independent terms that may be also included in the liquid-drop energy in order to improve the agreement with the experimental binding energies by accounting for some physical effects. The volume energy term is the largest, but since it is constant for a given nucleus the crucial shape dependence of E_{mac} resides in the functions B_S and B_C , describing the surface and Coulomb energies, respectively. They are crucial for the fission barriers and determine them nearly exclusively in medium-heavy nuclei, in which the macroscopic shape-dependent terms dominate the shell correction. The surface energy grows with deformation while the Coulomb energy decreases. The deformation-dependent curvature term turned out close to zero in some adjust-

ments of models to experimental masses, but it is present in the LSD macroscopic formula of [62].

There is another approach to macroscopic energy in which the surface and Coulomb energies from the outset include corrections for the surface diffuseness and/or finite range of interaction. A general way is to present them as double folding:

$$E = \int \int d^3\mathbf{r} d^3\mathbf{r}' \rho(\mathbf{r}) \rho(\mathbf{r}') f(\mathbf{r} - \mathbf{r}'), \quad (49)$$

where ρ are nucleon (or proton, for the Coulomb energy) densities and the function f models the interaction with a finite range. One can induce diffuseness in a sharp density, equal ρ_0 within the volume V_Σ , by folding it with a localized profile, like, for example, the Yukawa function:

$$g_Y(r_{12}) = \frac{1}{4\pi a^3} \frac{e^{-r_{12}/a}}{r_{12}/a}, \quad (50)$$

so that $\rho(\mathbf{r}_1) = \rho_0 \int_{V_\Sigma} d^3\mathbf{r}_2 g_Y(|\mathbf{r}_1 - \mathbf{r}_2|)$, where $r_{12}=|\mathbf{r}_1 - \mathbf{r}_2|$, a is the width of the Yukawa profile, and $\int d^3\mathbf{r} g_Y(\mathbf{r}) = 1$. Using g_Y as the nuclear interaction f and sharp surface densities one can model surface energy after subtracting from (49) the volume term. This approach was modified in [58] to the "Yukawa plus exponential" model which does not require any subtraction. The function $B_S(\Sigma)$ in this model is defined as:

$$B_S(\Sigma) = \frac{A^{-2/3}}{8\pi^2 r_0^2 a^4} \int \int_{V_\Sigma} \left(2 - \frac{r_{12}}{a}\right) \frac{e^{-r_{12}/a}}{r_{12}/a} d^3\mathbf{r}_1 d^3\mathbf{r}_2 \quad (51)$$

and was used in the Finite Range Liquid Drop Model (FRLDM) [54, 55, 56]. For charge densities folded with g_Y one can obtain from Eq. (49) the expression for the Coulomb energy [57]:

$$B_C(\Sigma) = \frac{15}{32\pi^2} \frac{A^{-5/3}}{r_0^5} \int \int_{V_\Sigma} \frac{1}{r_{12}} \left[1 - \left(1 + \frac{1}{2} \frac{r_{12}}{a_{den}}\right) e^{-r_{12}/a_{den}}\right] d^3\mathbf{r}_1 d^3\mathbf{r}_2, \quad (52)$$

also used in FRLDM. In the above formulas, $r_{12}=|\mathbf{r}_1 - \mathbf{r}_2|$, with \mathbf{r}_1 and \mathbf{r}_2 the positions of interacting volume elements, a - the range of the Yukawa interaction, a_{den} - the range of the Yukawa function used to generate nuclear charge distribution. The functions are normalized in such a way that they are equal 1 for a spherical nucleus in the limit of $a=0$ (for B_S) and $a_{den}=0$ (for B_C), corresponding to the traditional liquid-drop model with a sharp surface.

Phenomenological Deformed Potential

The phenomenological s.p. potential used to calculate shell correction energy is usually adjusted to the s.p. levels experimentally observed around Fermi energy in various nuclei. In order to reproduce observed magic shells it contains the spin-orbit part in addition to the central one and there is Coulomb potential for protons. Hence its general form may be written as follows:

$$V_{micr} = V_{centr} + \lambda \left(\frac{\hbar}{2mc} \right)^2 (\nabla V_{s.o.}) \cdot (\boldsymbol{\sigma} \times \mathbf{p}/\hbar) + V_C, \quad (53)$$

with the central potential V_{centr} , the spin-orbit potential $V_{s.o.}$, with m - nucleon mass, the s.o. strength λ , and the Coulomb potential for protons V_C . In general, the central and s.o. potentials for neutrons and protons are different.

Deformation of a nucleus is usually introduced to the s.p. potential in a similar way as in the macroscopic part - through a definition of the nuclear surface Σ via the equation involving deformation parameters, collectively designed β . The mostly used in the macro-micro methods are the folded Yukawa and the Woods-Saxon potentials.

The central part of the folded Yukawa potential is generated by the function g_Y with some chosen range a_p :

$$V_Y(\mathbf{r}) = -\frac{V_0}{4\pi a_p^3} \int_{V_\Sigma} \frac{e^{-|\mathbf{r}-\mathbf{r}'|/a_p}}{|\mathbf{r}-\mathbf{r}'|/a_p} d^3\mathbf{r}'. \quad (54)$$

The spin-orbit potential is the same as the central one, $V_{s.o.} = V_Y$. The potential depth V_0 , its radius defining the volume enclosed by the surface Σ and the spin-orbit strength λ are adjusted to data and depend on Z and N [55]. The Coulomb potential for protons is calculated for a uniform, sharp density $\rho_0 = Ze/(4\pi A r_0^3/3)$.

The Woods-Saxon potential which we use in our macroscopic - microscopic model is defined as follows. Its central part as given by S. Ćwiok et al [59] reads:

$$V_{WS}(\mathbf{r}) = -\frac{V}{1 + e^{d(\mathbf{r},\beta)/a_{ws}}}, \quad (55)$$

where V is the potential depth, $d(\mathbf{r},\beta)$ is the distance from the point \mathbf{r} to the surface of the nucleus Σ , taken with the plus sign outside, and minus inside Σ , a_{ws} is the diffuseness of the nuclear surface. For a spherical shape ($\beta = 0$), the function $d(\mathbf{r},\beta)$ reduces to: $r - R_0$ with a constant radius of a nucleus $R_0 = r_0 A^{1/3}$. The depth of the potential is

$$V = V_0(1 \pm \kappa I), \quad (56)$$

where $I = (N - Z)/A$, and V_0 and κ are adjustable parameters. The sign (+) is for protons and (−) for neutrons.

The full W-S potential has the form (53) with the spin-orbit part of the same form as V_{WS} , but with a different radius parameter. The radii and the s.o. strenghts are the

parameters of the model. The Coulomb potential is:

$$V_C(\mathbf{r}) = \rho_c \int_{V_\Sigma} \frac{d^3 r'}{|\mathbf{r} - \mathbf{r}'|}, \quad (57)$$

where $\rho_c = (Z - 1)e/(4\pi R_0^3/3)$ is the uniform charge density and the integration extends over the volume enclosed by the nuclear surface.

Search for Saddles

There are some points relevant to the application of the macro-micro method which are independent of the choice of the particular macro or micro model. Among them are those related to a search for fission saddles.

i) Which deformation parameters to use?

An arbitrary shape of a drop requires infinite number of coordinates. However, those of small wavelengths, close to the size of a nucleon, should be discarded as unphysical. Unfortunately, a reasonable cut off will depend on particular set of employed coordinates. Rather complete review of various deformation parametrizations used in studies of fission is given in [46]. The most used ones are: the parametrization by 3 matched quadratic surfaces and the one used here - the coefficients of expansion onto spherical harmonics. The first one is especially useful for elongated shapes close to scission and used by P. Möller et al to describe axially-symmetric shapes. The second one, used in our model, is general, but we avoid shapes without a symmetry plane. The nuclear surface Σ is defined by the equation for the surface radius as a function of spherical angles ϑ and φ [59]:

$$R(\vartheta, \varphi) = c(\{\beta\})R_0\left\{1 + \sum_{\lambda \geq 1} \beta_{\lambda 0} Y_{\lambda 0}(\vartheta, \varphi) + \sum_{\lambda \geq 1, \mu > 0} \beta_{\lambda \mu} Y_{\lambda \mu}^r(\vartheta, \varphi)\right\}, \quad (58)$$

where $c(\{\beta\})$ is the volume-fixing factor. The real-valued spherical harmonics $Y_{\lambda \mu}^r$ are defined in terms of the usual ones as: $Y_{\lambda \mu}^r = (Y_{\lambda \mu} + Y_{\lambda -\mu})/\sqrt{2}$ for μ even, and: $Y_{\lambda \mu}^r = -i(Y_{\lambda \mu} - Y_{\lambda -\mu})/\sqrt{2}$ for μ odd. In other words, we can treat shapes with one symmetry plane yz . Usually, however, we deal with shapes having two symmetry planes for which $\beta_{\lambda \mu} = 0$ for μ odd.

ii) How many deformations are sufficient?

At present, the practical restrictions by available computation resources confine one to 5 - 6 coordinates when performing calculations for many nuclei, which is about the minimal number necessary to describe shapes from the ground state to beyond the second barrier. This practically forces one to use different parametrization when describing ground states and different saddles.

iii) How to represent many-dimensional landscapes?

Any n -dimensional landscape with $n \geq 3$ is difficult to visualize. For a long time, two-dimensional energy maps serving the search for fission saddles were obtained by minimizing over the remaining, i.e. over the other $n - 2$, shape coordinates. This was an obvious and easiest choice, especially in the selfconsistent studies, which are based on the minimization with constraints. Unfortunately, such maps can distort reality if there are multiple minima in those $n - 2$ coordinates. An example is provided in Fig. 3. It follows that so obtained maps may be misleading as to the situation of fission saddles.

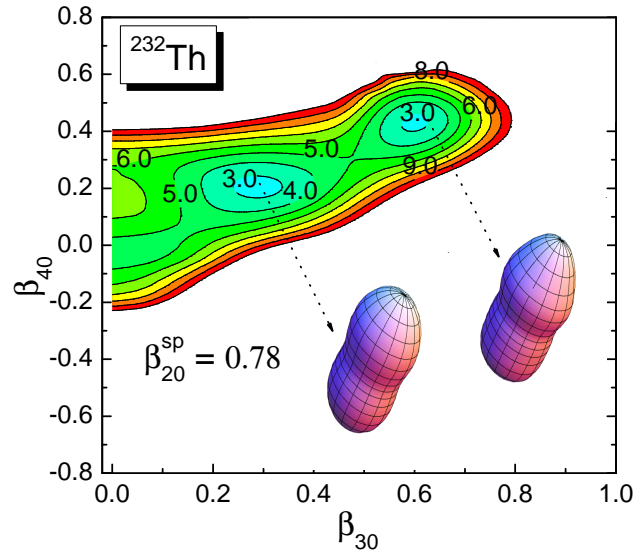


Fig. 3 Fragment of the energy surface for ^{232}Th projected on the (β_{30}, β_{40}) plane by fixing $\beta_{20} = 0.78$ and minimizing over $\beta_{50}, \beta_{60}, \beta_{70}, \beta_{80}$; the minima correspond to shapes lying slightly beyond the second saddle. Taken from [88]; copyright 2012 by APS.

iv) How to search for saddles?

Saddles on the energy landscape are neither minima nor maxima, therefore a proper method of search for them is required, different from the minimization. The fallacy of the minimization method with constraints in finding fission saddles was discussed on examples in [63, 64] and [65]. The related errors are also present in selfconsistent HFB or HF+BCS studies, see e.g. [66], where their elimination would require much more laborious calculations.

Two of possible correct methods are the "Dynamic Programming Method" used by A. Baran in the context of finding the subbarrier least action trajectory [67, 68] and the "Imaginary Water Flow" (IWF) borrowed from geographical topography studies, first used for finding fission barriers in [60]. Both start from calculating energies on a n -dimensional grid of deformations, of which one, say the first, q_1 , controls the elongation of the nucleus. Points (q_1, q_2, \dots, q_n) , with q_1 fixed and other q_i taking all possible values, form hypersurfaces enumerated by increasing values of q_1 . The first method aims at minimizing some functional over paths in consecutive steps: keeping the calculated optimal functional values for each point of the hypersurface k it updates the optimal values for each point of the next hypersurface $k + 1$. If one chooses the maximal energy on a path $V_{\max}(\text{path})$ as the functional, then its minimization over paths will give the fission barrier, see (1). In the second method, one simulates a gradual filling of the minimum with water and looks for a point at which the water starts to overflow to the neighbouring valley. Both methods require rather small mesh size and large memory, but the second one is more efficient and can treat up to six-dimensional grids in systematic calculations (8D for a single nucleus). Both have to be properly modified if there are many saddles - each of the saddles should be found and a selection procedure must be applied to choose the one defining the fission barrier height.

Specifications of the Model

The results which will illustrate some applications of the macro-micro method were obtained, unless stated otherwise, within the model specified in the recent work [71]. The macroscopic energy included surface and Coulomb terms given by Eq. (51,52), and parameters specified in [71]. The volume integrals in B_S and B_C , after turning them into surface integrals, were calculated by using the four-fold (or three-fold, for the axially symmetric shapes) N -point Gauss quadrature with $N \geq 64$. The deformed W-S potential was used as the phenomenological mean field, with the "universal" set of parameters given in [59]. The s.p. energies were calculated by using $n_p = 450$ lowest proton and $n_n = 550$ neutron levels from $N_{\max} = 19$ lowest shells of the deformed harmonic oscillator. The shell correction was calculated with the smoothing parameter $\bar{\gamma} = 1.2 \times 41/A^{1/3}$ MeV and the sixth-order polynomial ($p = 6$) for f_p . The pairing strengths: $G_n = (17.67 - 13.11 \cdot I)/A$ for neutrons, $G_p = (13.40 + 44.89 \cdot I)/A$ for protons ($I = (N - Z)/A$), as adjusted in [72], were used when solving the BCS equations including the lowest N (doubly degenerate) neutron and Z proton levels. The same parameters of the model were used previously in all our calculations of masses [71] and fission barriers [73, 74] of actinides and superheavy nuclei.

For odd and odd-odd nuclei, at each deformation, the energy minimization was performed over configurations of the odd particle, from the 10-th s.p. level below to the 10-th above the Fermi level. Pairing was included using the BCS with blocking. This means that we were looking for adiabatic saddle points in these nuclei.

After energy was calculated on a 5 - 7 dimensional deformation grid for each nucleus (see next section), the IWF procedure was applied to find fission saddles and select those which determine barrier heights.

Fission Barriers in Actinides

Fission barriers in actinide nuclei, which result from addition of deformation-dependent macro and micro terms of similar magnitude, exhibit a two-hump structure with both humps 5-6 MeV high in U or Pu, with the second one decreasing with Z , $B_B(\text{Th}) - B_B(\text{Cf}) > 2\text{MeV}$. Their structure was revealed by the discovery of fast fissioning states by Polikhanov et al. [43] and explained within the shell correction method by Strutinsky [39]. The explanation is that these are the ground, and sometimes also excited, states in the second well at large deformation and energy E_{II}^* above the g.s., and therefore protected from fission only by the second barrier reduced by E_{II}^* , $B_B - E_{II}^*$. Hence the name: shape- or fission isomers. The short fission half-lives of 10 ps - 10 ms make their study quite difficult.

The decrease in the second barriers has the exponential effect on spontaneous fission rates/half-lives, for example: $T_{1/2}^{sf} \approx 10^{19}$ yr for ^{235}U , 10^{14} yr for ^{241}Am , 86 yr for ^{252}Cf and 8 s for ^{252}No . At the same time, the height of the fission barrier in these nuclei is similar to the energy of separation of one neutron. Some actinide isotopes are fissile - they fission after a capture of thermal (i.e. with nearly zero kinetic energy) neutron. Applications of this phenomenon, first military but later also some peaceful, triggered many experimental studies of the induced fission which provided the current knowledge about the parameters of the barriers in actinides.

It is important to mention that the method of extracting heights and other parameters of the fission barriers from experiments is based on the one-dimensional picture of Fig. 1, see e.g. [42]. This adds to the uncertainty of comparisons between the quantity B defined above in terms of the multi-dimensional model and the "experimental" values reported usually as a result of fitting the excitation function in the neutron-induced reaction. One has also to mention that two sets of evaluated fission barriers in actinides differ for some nuclei by more than 0.5 MeV.

As followed from numerous studies [75, 76], shapes of actinide nuclei characteristic of primary (g.s.) and secondary (shape-isomeric) minima and fission saddles belong to different symmetry classes. The minima are axially symmetric, with reflection-asymmetric shapes showing only in ground states of very light isotopes. They were found by performing the energy minimization over deformations $\beta_{20}-\beta_{80}$ using the conjugate gradient method. To avoid falling into local minima, the minimization was repeated dozens of times for each nucleus with randomly selected starting deformations. For odd- Z or/and odd- N systems, the minimization over configurations was performed at every step of the gradient procedure.

The comparison of calculated and measured excitation energies E_{II}^* of isomeric minima in 28 actinide nuclei, mostly Pu, Am and Cm isotopes, shows that our calculation underestimates them by 0.3 MeV on average, with the root-mean-square (rms)

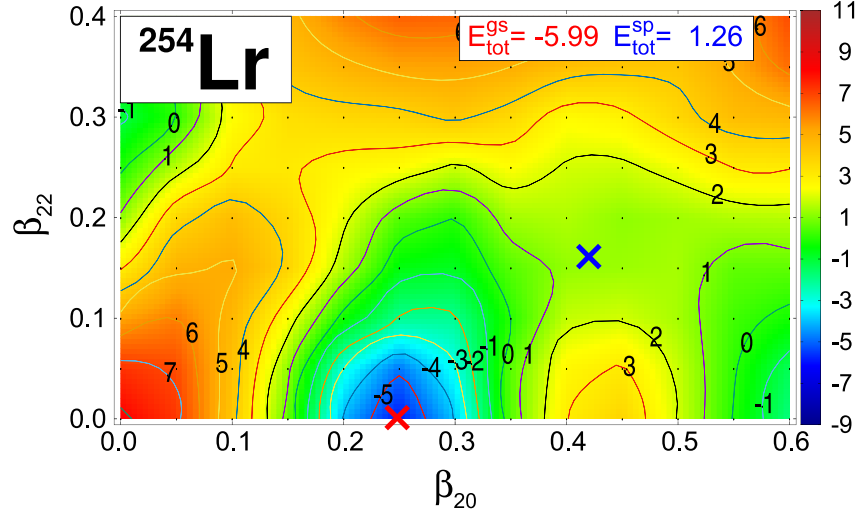


Fig. 4 Energy map in (β_{20}, β_{22}) plane for ^{254}Lr obtained by minimization over three remaining shape parameters $(\beta_{40}, \beta_{60}, \beta_{80})$; energy (in MeV) is relative to the macroscopic energy at the spherical shape.

deviation of 0.53 MeV, and the largest difference of 1.1 MeV. One has to notice that the measured values have often uncertainty of 0.2 - 0.4 MeV. The deformations β_{20} of secondary minima are between 0.5 and 0.80 and grow with A .

First and Second Barriers

One has to note that deformations of the first and even second fission saddles in actinides, although much larger than in their ground states, are still far from that of the scission configuration of two nearly disjoint fragments. Therefore, one can hope to describe them in terms of a relatively limited number of deformations $\beta_{\lambda\mu}$. When reaching behind the second barriers, one should check the reliability of the applied shape variety for the determination of the energy landscape, as the search for the third minima illustrates (see below).

The first barriers are very often considerably lowered by the nonaxiality [77, 78, 79, 80]. This is illustrated in Fig. 4, where we show the energy map in (β_{20}, β_{22}) plane for ^{254}Lr . One can see a substantially triaxial first saddle marked by the blue cross. On the other hand, the second barriers are considerably lowered by the reflection asymmetry - the fact which allowed Strutinsky to explain the puzzle of

asymmetric fission of actinides [81, 82]. Two examples are shown in Fig. 5, where energy maps in (β_{20}, β_{30}) plane are shown for ^{233}Th nad ^{251}Cf . One can see mass - asymmetric second saddles, a more pronounced in Th. This knowledge suggests using different deformation sets while searching for the first and the second barriers.

The first saddle points were searched by the IWF algorithm on the five-dimensional grid including even- λ deformations β_{20} - β_{80} , within the range of β_{20} : 0 - 0.60, and the quadrupole nonaxiality β_{22} - altogether 5 variables. The initial grid of 29250 points was fivefold interpolated to more than 50 million points to perform the IWF. The grid for the search of the second saddles used the same deformations as for minima, but for each point β_{20} - β_{80} (seven variables) the deformation β_{10} was added, determined by the center - of - mass condition. With β_{20} reaching 1.5, the seven-dimensional mesh contained ≈ 7.5 million points. As a two-fold interpolation did not modify the results of the IWF search we decided to find second saddles without any interpolation in this case.

The calculated first fission barriers are substantially too small for Th isotopes, close to the values evaluated from experiments for Pa and U, and too large on average for larger Z. The first effect, known as the "thorium anomaly" is common to many theoretical calculations and, perhaps, related to the barrier shapes different from those assumed in the analysis of experimental data. The second barriers, except for Th and the lightest isotopes of Pu and Cm, come out overestimated. Additionally, those for Pu and Am show an increase with N which does not exist in experiment, but shows up in many selfconsistent calculations. Both, the first and second barriers in our model show the odd-even staggering which is more pronounced than in experiment, to a degree which depends on which experimental set one uses for comparison. In Fig. 6 we present the calculated barriers vs experimental data for "well" and "not-so-well" agreeing with the data isotopic U and Am chains. The agreement with the "experimental" barriers for Am isotopes may be slightly improved by assuming larger by 5% pairing strength for odd-Z and odd- N nuclei. The corresponding barriers, calculated for the sake of test, are shown in orange in Fig. 6. Such change would slightly spoil the agreement of calculated nuclear masses with the experimental ones.

The present ability of the MM model to reproduce barrier heights in actinides may be illustrated by the obtained root-mean-square deviations from two existing sets of experimental estimates, including respectively 71 and 45 nuclei. For the first barriers they are: 0.94 (set I) and 0.85 MeV (set II), for the second barriers: 0.92 (set I) and 0.82 MeV (set II). Within the FRLDM of Möller et al [65] these deviations are quite similar for the second barriers, but sizably larger for the first [1.48 (set I) and 1.35 MeV (set II)].

Uncertain Third Minima and Barriers

Fission probabilities in neutron capture reactions on some actinides show narrow resonances at excitation energies above the second barrier. A fine structure of some

was interpreted as a signature of multiple hyperdeformed (i.e. having moments of inertia larger than in the isomeric minima) rotational bands. Interpretation was provided in terms of a (one dimensional) barrier with the third minimum and the third hump. Measurements of the angular distribution of the fission fragments at those excitation energies support this interpretation. Results for ^{232}Th were consistent with a relatively shallow 300 keV minimum [83, 84, 85]. Later experiments claimed much deeper third minima in a number of nuclei, including $^{234,236}\text{U}$, see [76] and references therein.

Theoretical selfconsistent calculations as well as earlier macro-micro results showed at most shallow third minima and, as shown in M. Kowal and J. Skalski [86], and P. Jachimowicz et al. [87], this is also the result of the present model. These minima correspond to quite elongated, reflection - asymmetric shapes whose description in the parametrization (58) already poses a problem. For their proper treatment it turned out necessary to explicitly include the dipole deformation β_{10} , which is spurious at small deformations for which it merely shifts the center of the shape. The effect of including β_{10} is illustrated in Fig. 7, 8, 9. The two, similarly looking shapes differing only by β_{10} shown in Fig. 7 correspond to quite different energies. The energy landscapes for ^{232}Th in Fig. 8, obtained with and without β_{10} , show a drastic reduction of the third barrier by β_{10} . This is also seen in Fig. 9, in which the barriers along a possible fission paths are shown.

It has to be emphasized that the effect of β_{10} on the second barrier in actinides is weak, as documented in two calculations by P. Jachimowicz et al. [88, 74].

Fission of K -isomers at the Second Minimum

One of the unsolved questions is how much of the symmetry of a given one-, two- or a few-quasiparticle configuration at the g.s. or secondary minimum is preserved along the barrier which controls its fission rate. This problem is relevant to fission rates of odd- A and odd-odd nuclei as well as high- K isomers. Nonaxial saddle deformations, like those at the first barriers in actinides, suggest that in their transmission the K quantum number is probably not preserved. An interesting case are the possible high- K isomers at the superdeformed second minima in actinides for which the axial symmetry of the second barrier would imply the conservation of the K quantum number in fission. That could lead to a substantial increase in the barrier height for such isomers.

In tables [90] one finds that in each even-even $^{240-244}\text{Cm}$ there were detected two isomeric fission half-lives differing by 3 - 4 orders of magnitude, with $T_1 = 40$ ps and $T_2 = 180$ ns in ^{242}Cm . Energy landscapes calculated for this nucleus around and beyond the second minimum are shown in Fig. 10 (taken from [89]) for the adiabatic (i.e. the lowest configuration at each deformation) and $K = 10$ configuration, dominantly two-neutron $\nu 11/2^+$, $\nu 9/2^-$ in the second well, which, according to the level scheme of the W-S potential, is the main candidate for a K -isomer there. It may be seen that a large increase in the height (≈ 4 MeV) and width

of the second fission barrier is predicted for the $K = 10$ configuration. If the situation presented in Fig. 10 is real, then the difference in fission half-lives T_1 and T_2 would rather come from a delay of the *electromagnetic* transition from the isomer to the g.s. in the second well (with the subsequent fission of the latter) than from the direct fission of the isomer, for which the increased fission barrier suggests a longer fission half-life.

Barriers in Superheavy Nuclei

While results in the actinide region can serve as a check the model's consistency with experimental data, calculations in the region of superheavy nuclei are predictions involving a serious extrapolation. One should bear in mind that this concerns all methods used, does not matter how 'realistic' or 'fundamental' they claim to be. The real issue at hand is the dependence of the mean-field or phenomenological potential on Z and N in the uncharted region of the table of isotopes. An uncertainty regarding this dependence is directly reflected in the uncertain next magic numbers beyond lead which come out differently in different models. Of course, issuing fission barriers are also strongly model - dependent, even if in the actinide region they were similar.

All calculated fission barrier heights within the presented MM approach were collected and shown as a map $B_f(Z, N)$ in Fig. 11. One can see three areas of clearly raised fission barrier: $(Z \approx 102, N \approx 152)$, $(Z \approx 108, N \approx 162)$, $(Z \approx 114, N \approx 180)$ and the region of low barriers around $N \approx 170$. The effect of the odd particle, i.e., an often (but not always) higher barrier in the neighbouring odd-particle system, can be seen in Fig. 11. Looking at this global set of barriers in the superheavy nuclei, one can conclude that in the whole region $Z = 98 - 126$ the predicted fission barriers are limited, $B < 8\text{MeV}$.

The categories of obtained saddle-point shapes are shown in Fig. 12, taken from ref [71]. As one can see, the saddles are mostly triaxial. The effect of the lowering of the axially-symmetric barrier by the quadrupole nonaxiality β_{22} , marked in red, is very systematic and affects almost 3/4 of all considered nuclei. The green color in Fig. 12 shows the mass-asymmetric saddle points. The nuclei having triaxial shapes at saddle points with additional hexadecapole nonaxiality β_{42} and β_{44} are marked by yellow dots. Here belong many neutron deficient nuclei with $Z \geq 119$.

For an additional insight, one can crosscheck barriers predicted within other models. We start with the comparison of the fission barriers for ^{266}Hs calculated in the frame of various models based on different methodologies. The barriers derived in the Skyrme HFB [92], Gogny HF [93] and the present MM model are shown in Fig. 13, taken from [70], as a function of the quadrupole moment Q_{20} . One can see that for this particular nuclide there is a relatively good agreement in barrier heights. The differences in the peak height (the saddle point) reach 1 MeV.

The main conclusion from Fig. 12 and 13 is that the effect of triaxiality is significant in all models and *should not* be ignored. Therefore, we have chosen for a more

systematic comparison/discussion only the models that take this effect into account. Furthermore, while all models predict similar barrier heights in the area of the element Hs, they differ considerably for much heavier nuclei. It is clearly visible in Fig. 14 for nuclei with $Z = 114$ and $Z = 120$.

For Flerovium isotopes, the barriers calculated by the MM model and with the SKM* interaction [92] agree with the experimental (empirical) estimates [95]. The FRLDM [91] overestimates these quasi-empirical barriers [95] significantly. Although only the lower limit for the barrier height has been estimated in [95], which would reproduce the known fusion cross-sections at the picobarn level, such a high barrier seems problematic. On the other hand, with small barriers obtained within the RMF model, one cannot explain the experimentally known millisecond fission half-life in ^{284}Fl . One should note, however, that a slight tuning of the RMF model [96] gives higher barriers, closer to the MM results presented here.

For $Z = 120$ the MM results are very close to those obtained within the RMF model, see Fig. 14. The results of [91] are systematically higher by ≈ 1 MeV. This is in contrast with the Skyrme SkM* prediction [92] of the high barriers for $Z = 120$ [92], related to the proton magic gap. Three models: FRLDM, RMF and MM converge to $B_f \simeq 5$ MeV at $N = 182\text{--}184$. The nucleus $^{302}120$ is particularly interesting, as two unsuccessful attempts to produce it have already taken place in GSI, providing a cross-section limit of 560 fb [97] or 90 fb in [98], and in Dubna [99], providing the limit of 400 fb. The cross-section estimates [100] do not support a possibility of easy production of this SH isotope in the laboratory. However, with the barrier of the order of 10 MeV, as obtained in the frame of the self-consistent Skyrme SkM* theory, producing superheavy $Z = 120$ nuclei, it seems, should not pose any difficulties.

Conclusions

Nuclear fission is an extremely complex process, difficult to analyse within a genuinely microscopic quantum theory. In order to gain a qualitative understanding of it and obtain quantitative estimates of experimentally measured observables we use a number of concepts, like the nuclear deformation and the fission barrier or, more generally, energy landscape. Although not directly measurable, they provide clues about physics of fission, are ingredients in formulas for probabilities of various reactions and decays and give hints concerning the synthesis and detection of the heaviest nuclei.

The ingenious method of shell correction by Strutinsky allowed to bypass severe limitations of microscopic theories and calculate in a relatively simple manner energy landscapes of nuclei with an acceptable error. Although large selfconsistent mean-field calculations are possible today, the macro-micro method is still competitive in areas like nuclear fission, in which it is necessary to account for all important deformations in hundreds or more nuclei, including odd and odd-odd, which multiplies the numerical effort.

The presented results of the macro-micro model illustrate the status of agreement between the calculated and evaluated from experiment fission barriers in 72 actinides, in which they are known. In view of the uncertainties, both in experimental evaluations and in the macro-micro method, the obtained agreement seems reasonable. A slightly worse agreement was obtained in the FRLDM model, which encompasses much larger number of nuclei, while the selfconsistent results in actinides are of very mixed quality, and nearly always missing the odd and odd-odd nuclei.

The calculated fission barriers in superheavy nuclei constitute a predictive part of the present chapter. They are compared to the results of other calculations, including the selfconsistent ones, and the differences between models are shortly discussed. These differences are strongly related to our ignorance as to the next magic numbers beyond lead, especially the one for protons. The large differences in predictions mean that experiment will eliminate some of the models someday.

References

1. O. Hahn, F. Strassmann, *Naturwissenschaften* **27**, 11 (1939).
2. K. A. Petrzhak, G. N. Flerov, *Proc. USSR Acad. Sci.* **28** (6), 500 (1940); G. N. Flerov, K. A. Petrzhak, *Phys. Rev.* **58**, 89 (1940).
3. L. Meitner, O. R. Frisch, *Nature (London)* **143**, 239 (1939).
4. N. Bohr, *Nature* **143**, 330 (1939).
5. N. Bohr, J. A. Wheeler, *Phys. Rev.* **56**, 426 (1939).
6. G. Gamow, *Proc. R. Soc. London, Ser. A* **126**, 632 (1930).
7. J. H. van't Hoff, "Etudes de Dynamiques Chimiques" (F. Muller & Co., Amsterdam, 1884), p. 115
8. S. Arrhenius, *Z. Phys. Chem.* **4**, 226 (1889).
9. L. Landau, *Phys. Z. Sowjetunion* **1**, 88. (1932); C. Zener, *Proc. R. Soc. (Lond.) A* **137**, 696 (1931); E. C. G. Stückelberg, *Helv. Phys. Acta* **5**, 369. (1932).
10. D. L. Hill and J. A. Wheeler, *Phys. Rev.* **89**, 1102 (1953).
11. G. Schütte G and L. Wilets Excitation during collective deformation: How simple it is *Z. Physik A* **286**(3), 313–318. (1978).
12. W. Nazarewicz, *Nuclear Physics A* **557** (1993).
13. P. Jachimowicz, M. Kowal, and J. Skalski, *Phys. Rev. C*, **92**, 044306 (2015).
14. E. Wigner, *Trans. Faraday Soc.* **34**, part1, 29 (1938).
15. L. D. Landau, E. M. Lifshitz, *Statistical Physics, Part 1*, 3rd edition by E. M. Lifshitz, L. P. Pitaevski, (Pergamon, Oxford, 1980).
16. H. A. Kramers, *Physica (Amsterdam)* **7** 284 (1940).
17. H. Feldmeier *Rep. Prog. Phys.* **50** 915 (1987).
18. P. Hänggi, P. Talkner, M. Borkovec, "Reaction-rate theory: fifty years after Kramers.", *Rev. Mod. Phys.*, **62**, (1990).
19. "New Trends in Kramers' Reaction Rate Theory" Edited by P. Talkner P. Hänggi, © 1995 Springer Science+Business Media Dordrecht Originally published by Kluwer Academic Publishers in (1995). DOI 10.1007/978-94-011-0465-4
20. P. Fröbrich and R. Lipperheide, "Theory of Nuclear Reactions.", Oxford University Press Inc., New York, ISBN 0 19 853783 2, (1996).
21. S. Bjørnholm and J. E. Lynn *Rev. Mod. Phys.* **52**, 725 (1980).
22. A. Sobiczewski, Z. Szymanski, S. Wycech, S. G. Nilsson, J. R. Nix, C. F. Tsang, C. F. Gustafson, P. Möller, and B. Nilsson, *Nucl. Phys. A* **131**, 69, (1969).

23. H. Krappe and K. Pomorski, Theory of Nuclear Fission (Springer, 2012).
24. M. Sin and R. Capote, *Phys. Rev. C* **77**, 054601 (2008).
25. M. Sin, R. Capote, M. W. Herman, A. Trkov, *Phys. Rev. C* **93** 034605, (2016).
26. S. Goriely, S. Hilaire, A. J. Koning, M. Sin, and R. Capote *Phys. Rev. C* **79**, 024612 (2009).
27. S. Hilaire, J.P. Delaroche, and M. Girod, *Eur. Phys. J. A* **12**, 169–184 (2001).
28. S. Goriely, S. Hilaire, and A. J. Koning, *Phys. Rev. C* **78**, 064307 (2008).
29. A.H. Blin *et al.*, *Nucl. Phys. A* **456**, 109 (1986).
30. H. Uhrenholt, S. Åberg, A. Dobrowolski, Th. Døssing, T. Ichikawa, and P. Möller, *Nucl. Phys. A* **913**, 127 (2013).
31. S. Åberg, B.G. Carlsson, Th. Døssing, and P. Möller, *Nucl. Phys. A* **941**, 97 (2015).
32. D.E. Ward, B.G. Carlsson, Th. Døssing, P. Möller, J. Randrup, and S. Åberg, *Phys. Rev. C* **95**, 024618 (2017).
33. M. Albertsson, B.G. Carlsson, Th. Døssing, P. Möller, J. Randrup, and S. Åberg, *Phys. Lett. B* **803**, 135276 (2020).
34. B. Nerlo-Pomorska, K. Pomorski, J. Bartel, and K. Dietrich, *Phys. Rev. C* **66**, 051302(R) (2002).
35. R. A. Senkov and M. Horoi, *Phys. Rev. C* **82**, 024304 (2010).
36. Y. Alhassid, M. Bonett-Matiz, S. Liu, and H. Nakada *Phys. Rev. C* **92**, 024307 (2015).
37. A. Rahmatinejad, A. N. Bezbakh, T. M. Shneidman, G. Adamian, N. V. Antonenko, P. Jachimowicz, and M. Kowal *Phys. Rev. C* **103**, 034309 (2021).
38. W. Swiatecki, *Phys. Rev.* **100**, 937 (1955).
39. V. M. Strutinsky, *Nucl. Phys. A* **95**, 420 (1967).
40. V. M. Strutinsky, *Nucl. Phys. A* **122**, 1 (1968).
41. M. Brack, J. Damgaard, A. S. Jensen, H. C. Pauli, V. M. Strutinsky, C. Y. Wong, *Rev. Mod. Phys.* **44**, 320 (1972).
42. R. Capote *et al.*, *Nucl. Data Sheets* **110** 3107 (2009).
43. S. M. Polikhanov *et al.*, *Sov. Phys. JETP* **15** 1016 (1962).
44. G. N. Flerov, V. A. Druin, JINR preprint R-2539, Dubna, 1966 (unpublished) (1966).
45. G. N. Smirenkin, IAEA Report No. INDC(CCP)-359, Vienna, (1993).
46. R. W. Hasse, W. D. Myers, *Geometrical Relationships of Macroscopic Nuclear Physics* (Springer, Berlin, Heidelberg, 1988).
47. W. Nazarewicz, T. R. Werner, J. Dobaczewski, *Phys. Rev. C* **50**, 2860 (1994).
48. N. Tajima, Y. R. Shimizu, S. Takahara, *Phys. Rev. C* **82**, 034316 (2010).
49. T. Vertse, A. T. Kruppa, R. J. Liotta, W. Nazarewicz, N. Sandulescu, T. R. Werner, *Phys. Rev. C* **57**, 3089 (1998).
50. A. T. Kruppa, *Phys. Lett. B* **431**, 237 (1998).
51. S. Shlomo, V. M. Kolomietz, and H. Dejbakhsh *Phys. Rev. C* **55**, 1972 (1997).
52. T. Vertse, A. T. Kruppa, W. Nazarewicz, *Phys. Rev. C* **61**, 064317 (2000).
53. B. Mohammed-Azizi, *Phys. Rev. C* **100**, 034319 (2019).
54. P. Möller, J. R. Nix, *Atomic Data and Nuclear Data Tables* **26**, 165 (1981).
55. P. Möller, J. R. Nix, W. D. Myers, W. Swiatecki, *At. Data and Nucl. Data Tables* **59**, 185 (1995).
56. P. Möller, A. J. Sierk, T. Ichikawa, H. Sagawa, *At. Data and Nucl. Data Tables* **109-110**, 1 (2016).
57. K. T. R. Davies, J. R. Nix, *Physical Review C* **14**, 185 (1977).
58. H. J. Krappe, J. R. Nix, A. J. Sierk, *Physical Review C* **20**, 992 (1979).
59. S. Ćwiok, J. Dudek, W. Nazarewicz, J. Skalski, and T. Werner, *Comput. Phys. Commun.* **46**, 379 (1987).
60. A. Mamdouh, J. M. Pearson, M. Rayet, F. Tondeur, *Nucl. Phys. A* **644** 389 (1998).
61. W. J. Swiatecki, *Nucl. Phys. A* **574** 233 (1994).
62. K. Pomorski and J. Dudek *Phys. Rev. C* **67**, 044316 (2003).
63. W. D. Myers, W. Swiatecki, *Nucl. Phys. A* **601** 141 (1996).
64. P. Möller, A. Iwamoto, *Physical Review C* **61**, 047602 (2000).
65. P. Möller, A. J. Sierk, T. Ichikawa, A. Iwamoto, R. Bengtsson, H. Uhrenholt, S. Åberg, *Physical Review C* **79**, 064304 (2009).

66. N. Dubray, D. Regnier, *Comput. Phys. Commun.* **183** 2035 (2012).
67. A. Baran, *Phys. Lett. B* **76**, 8 (1978).
68. A. Baran, K. Pomorski, A. Lukasiak, A. Sobiczewski *Nuclear Physics A*, **361**, 1 (1981).
69. R. Vandenbosch and J. R. Huizenga, *Nuclear fission*, (Academic Press, New York, 1973).
70. A. Baran, M. Kowal, P.-G. Reinhard, L. M. Robledo, A. Staszczak, and M. Warda, *Nucl. Phys. A* **944**, 442 (2015).
71. P. Jachimowicz, M. Kowal, J. Skalski, *Atomic Data and Nuclear Data Tables* **138** 101393 (2021).
72. I. Muntian, Z. Patyk, and A. Sobiczewski, *Acta Phys. Pol. B* **32**, 691 (2001).
73. P. Jachimowicz, M. Kowal, and J. Skalski, *Phys. Rev. C* **95**, 034329 (2017).
74. P. Jachimowicz, M. Kowal, and J. Skalski, *Phys. Rev. C* **101**, 014311 (2020).
75. P. G. Thirolf and D. Habs, *Prog. Part. Nucl. Phys.* **49**, 325 (2002); P. Thirolf, D.Dc. Thesis, Ludwig-Maximilians-Universitat München (2003).
76. A. Krasznahorkay, in *Handbook of Nuclear Chemistry* (Springer-Verlag, Berlin, 2011), p. 281.
77. V. V. Pashkevich, *Nucl. Phys. A* **133**, 40 (1969).
78. S. E. Larsson, I. Bagnarsson, and S. G. Nilsson, *Phys. Lett. B* **38**, 263 (1972).
79. H. Schultheiss, and R. Schultheiss, *Phys. Lett. B* **34**, 245 (1971).
80. S. E. Larsson, G. Leander, I. Bagnarsson, and J. Randrup, *Phys. Scr. A* **10**, 65 (1974).
81. P. Möller and S. G. Nilsson, *Phys. Lett. B* **31**, 283, (1970).
82. P. Möller, *Nucl. Phys. A* **192**, 529 (1972).
83. J. Blons et al., *Phys. Rev. Lett.* **35**, 1749 (1975).
84. J. Blons et al., *Nucl. Phys. A* **502**, 121c (1989).
85. J. Blons et al., *Nucl. Phys. A* **477**, 231 (1988).
86. M. Kowal and J. Skalski *Phys. Rev. C* **85**, 061302(R) (2012).
87. P. Jachimowicz, M. Kowal, J. Skalski, *Phys. Rev. C*, 044308 (2013).
88. P. Jachimowicz, M. Kowal, J. Skalski, *Phys. Rev. C* **85**, 034305 (2012).
89. W. Brodziński, M. Kowal, J. Skalski, P. Jachimowicz, *Acta Phys. Pol. B* **49**, 621 (2018).
90. B. Singh, R. Zywina, R. Firestone, *Nuclear Data Sheets* **97**, 241 (2002)
91. P. Moller, A. J. Sierk, T. Ichikawa, A. Iwamoto, and M. Mumpower, *Phys. Rev. C* **91**, 024310 (2015).
92. A. Staszczak, A. Baran, and W. Nazarewicz: *Phys. Rev. C* **87** (2013) 024320.
93. M. Warda, J.L. Egidio *Phys. Rev. C* **86**, 014322 (2012).
94. H. Abusara, A. V. Afanasjev, and P. Ring: *Phys. Rev. C* **85** (2012) 024314; **C 82** (2010) 044303.
95. M.G. Itkis, Y.T. Oganessian, V.I. Zagrebaev, *Phys. Rev. C*, **65**, 044602 (2002).
96. A.V. Afanasjev, S.E. Agbemava, *Acta Physics Polonica*, **B 46**, (2015).
97. S. Hofmann et al., *GSI Sci. Rep.*, p. 205 (2015).
98. S. Hofmann, *Russ. Chem. Rev.* **78**, 1123 (2009).
99. Oganessian, Yu.Ts. Utyonkov, V. Lobanov, Yu. Abdullin, F. Polyakov, A. Sagaidak, R. Shirokovsky, I. Tsyganov, Yu. et al. (2009). *Phys. Rev. C* **79** (2) (2009).
100. K. Siwek-Wilczyńska, T. Cap, and J. Wilczyński, *Int. J. Mod. Phys. , E***19**,500 (2010).

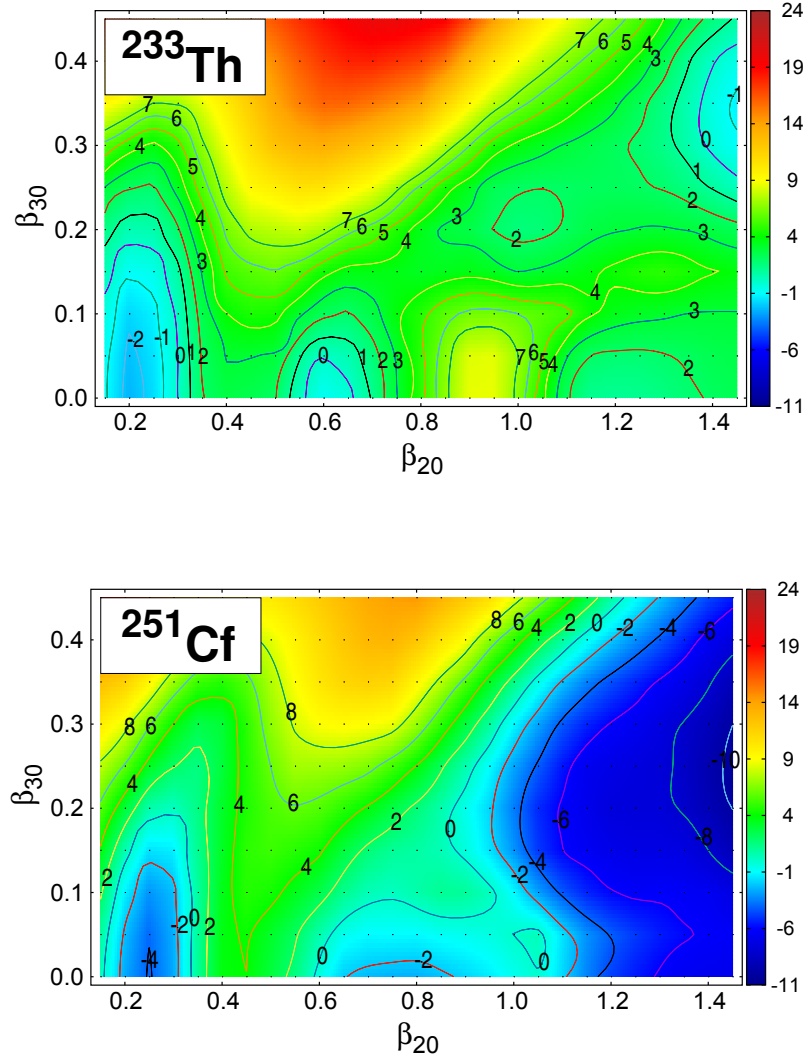


Fig. 5 Energy maps in (β_{20}, β_{30}) plane for ^{233}Th and ^{251}Cf obtained by minimization over five remaining shape parameters $\{\beta_{40}, \beta_{50}, \beta_{60}, \beta_{70}, \beta_{80}\}$ with β_{10} fixed at each point by the center-of-mass condition; energy (in MeV) is given relative to the macroscopic energy at the spherical shape. Taken from [74]; copyright 2020 by APS.

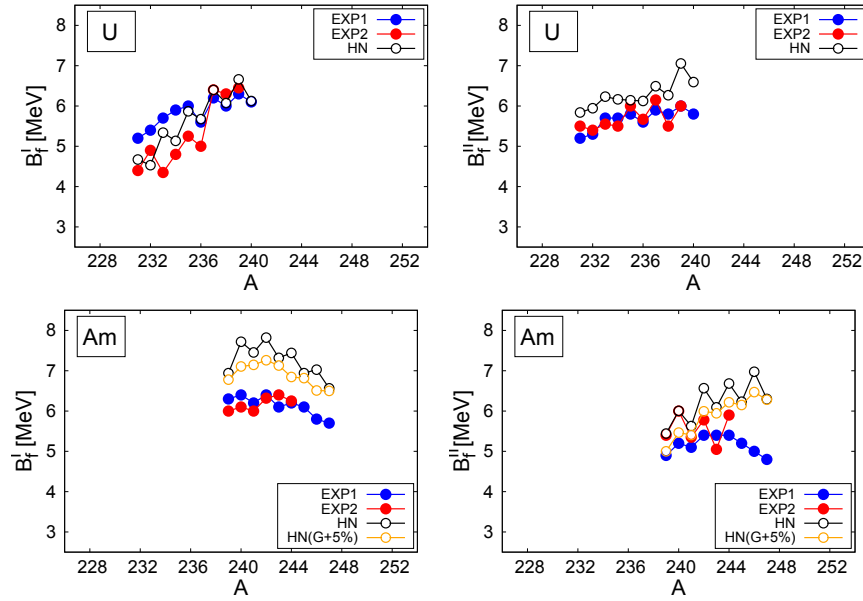


Fig. 6 First and second fission barrier heights in uranium and americium nuclei: results of the present model (black circles) and experimental (G. N. Smirenkin 1993) (red dots) and (Capote et al 2009) (blue dots). For americium nuclei, the effect of 5% enhanced pairing was additionally shown (open orange circles) Taken from [74]; copyright 2020 by APS.

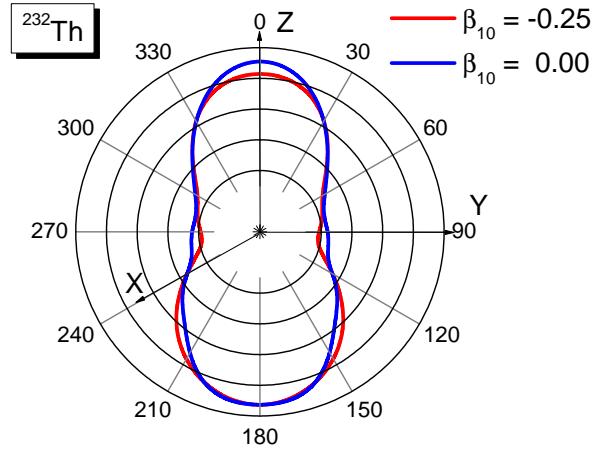


Fig. 7 Influence of the β_1 deformation on the nuclear shape. Taken from [87]; copyright 2013 by APS.

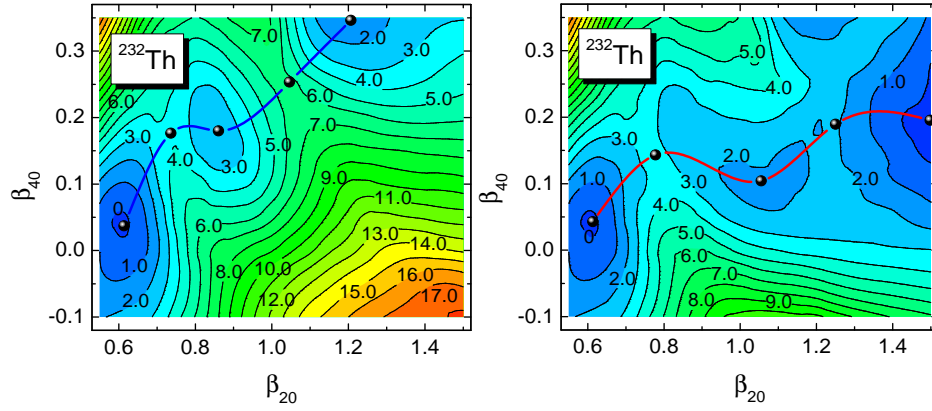


Fig. 8 Effect of β_1 on the energy surface of ^{232}Th ; two paths through the barrier correspond to shapes constructed by omitting (blue) and using (red) deformation β_{10} . Taken from [87]; copyright 2013 by APS.

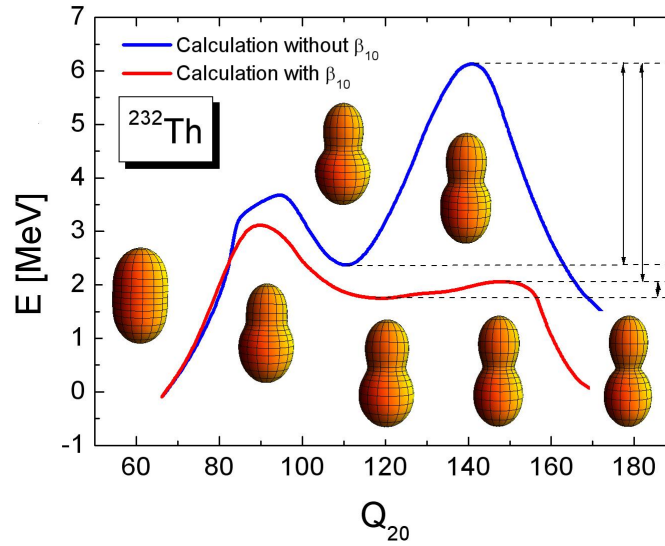


Fig. 9 Effect of β_1 on the effective one-dimensional barrier in ^{232}Th shown as a function of quadrupole mass moment. Taken from [87]; copyright 2013 by APS.

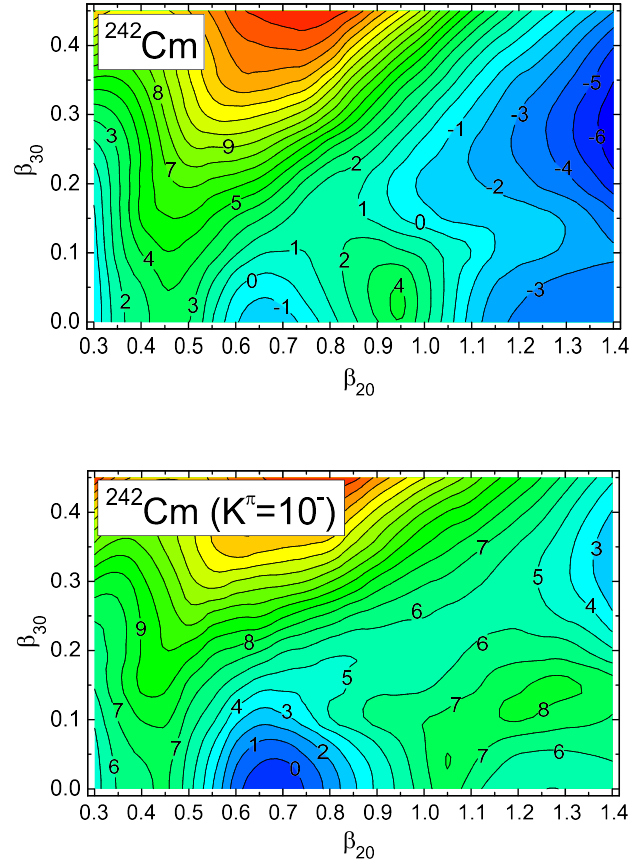


Fig. 10 Energy relative to the macroscopic energy at the spherical shape in (β_{20}, β_{30}) plane for the lowest and $K^\pi = 10^-$ configuration in ^{242}Cm around and beyond the second minimum, obtained by minimization over remaining coordinates β_{40} - β_{80} . The effect of keeping configuration on the fission barrier may be clearly seen. Taken from [89]; copyright 2018 by APB.

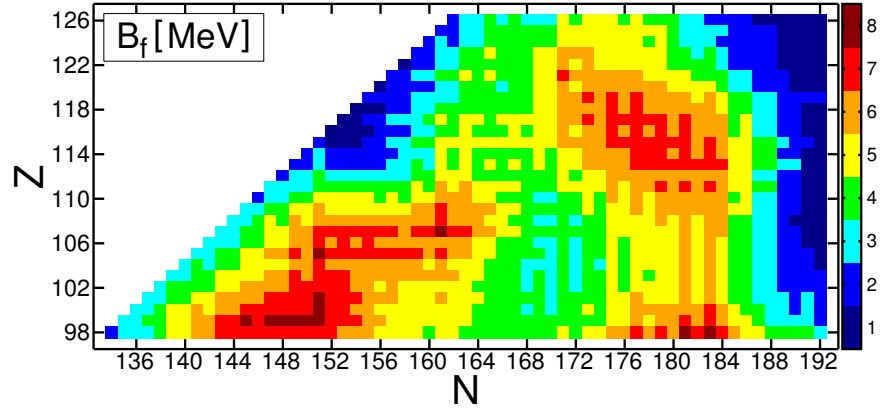


Fig. 11 Calculated fission barriers B_f for superheavy nuclei according to MM model described in this Chapter. Figure taken from [73]; copyright 2017 by APS.

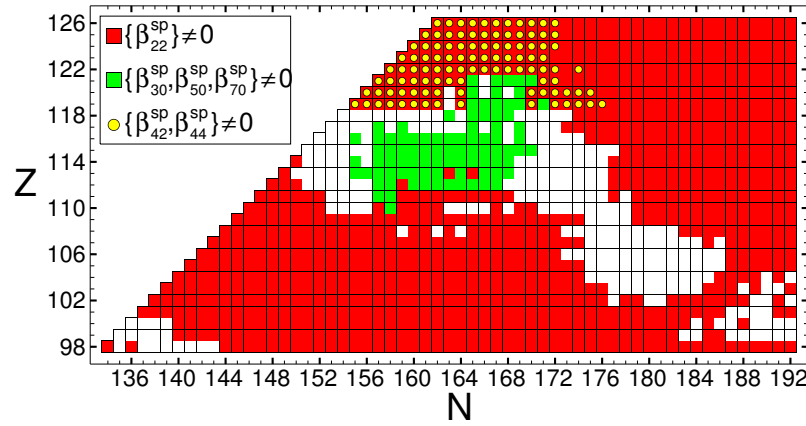


Fig. 12 Nuclei with β_{22} deformation at the saddle point (red squares), mass-asymmetric fission saddle point (green squares) and saddles with nonaxial hexadecapole deformation (yellow circles). White regions in the considered area denotes nuclei with axially- and reflection- symmetric saddle point [71]; copyright 2021 by Elsevier.

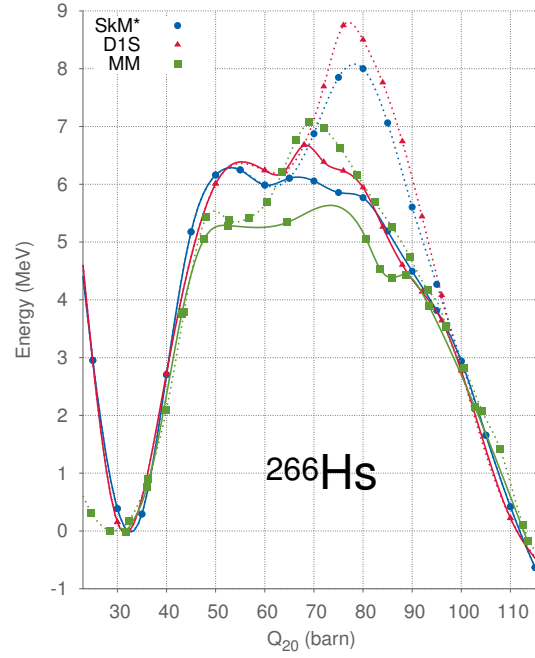


Fig. 13 Fission barrier of ^{266}Hs as function of the quadrupole moment Q_{20} calculated in MM model (green, filled squares), Skyrme HFB approach (blue, filled circles) and Gogny HF model (red, filled triangles). Dashed lines represent the raw axial barrier. Solid lines correspond to the barriers with triaxiality - γ . Taken from [70]; copyright 2015 by Elsevier.

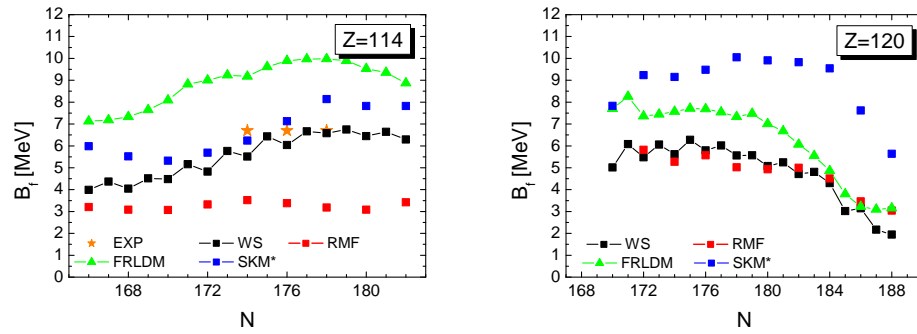


Fig. 14 Fission barriers predicted by various models: black - WS model, green – FRLDM [91], blue – SkM* [92], red – RMF with NL3 parametrization [94] and experimental data taken from [95] for $Z=114$ (left panel) and for $Z=120$ (right panel) isotopes. Taken from [73]; copyright 2017 by APS.